



Palaeoliquefaction features in Baltic Ice Lake sediments: A case study from Western Latvia

Małgorzata Pisarska-Jamroży ^a, Szymon Belzyt ^b, Māris Nartišs ^c, Albertas Bitinas ^d, Barbara Woronko ^e, Alar Rosentau ^f, Szymon Świątek ^{a,*}

^a Institute of Geology, Adam Mickiewicz University, Krygowskiego 12 Street, 61-680, Poznań, Poland

^b Institute of Geological Sciences, University of Wrocław, Pl. Maksa Borna 9, 50-204, Wrocław, Poland

^c Department of Geography, Faculty of Science and Technology, University of Latvia, Jelgavas str. 1, Riga, LV-1004, Latvia

^d State Scientific Research Institute Nature Research Centre, Akademijos Street 2, 08412, Vilnius, Lithuania

^e University of Warsaw, Faculty of Geology, Żwirki i Wigury Street 93, 02-089, Warsaw, Poland

^f Department of Geology, University of Tartu, Ravila 14A, 50411, Tartu, Estonia

ARTICLE INFO

Keywords:

Nearshore
Soft-sediment deformation structures
Liquefaction
Fluidisation
Storm and wave action
Overloading
Microstructural analysis
Microsedimentology
Late Pleistocene

ABSTRACT

Studies of liquefaction features in sedimentary archives offer valuable insights into past deformation processes. This study investigates palaeoliquefaction-induced soft-sediment deformation structures (SSDS) preserved within Late Pleistocene nearshore deposits at the Sārnate site in western Latvia, formed during the Baltic Ice Lake. Sedimentological, microstructural, and geochronological analyses were employed to reconstruct depositional conditions and constrain the timing of deformation events. Changes in depositional environments associated with the Baltic Ice Lake, specifically the transition from deeper to shallower water at the study site, were likely driven by the drainage of the Baltic Ice Lake. This may have created conditions conducive to liquefaction and fluidisation, leading to sediment destabilisation and the formation of SSDS, like injection structures, load structures (load casts, pseudonodules) and flame structures. These environmental shifts likely increased pore water pressure within the heterolithic deposits, composed of alternating coarse and fine sediments, rendering them more prone to liquefaction. Liquefaction and the resulting SSDS in these water-saturated nearshore deposits were primarily triggered by overloading, which exerted additional, uneven pressure on the underlying layers, thereby enhancing their liquefaction potential. This process was likely intensified by storm and wave activity. Our findings highlight the critical role of site-specific sedimentological characteristics in influencing liquefaction susceptibility and deformation styles. The spatial distribution, morphology, and textural features of the observed SSDS, indicate past episodes of sediment deformation driven by water level changes in the Baltic Ice Lake. These insights contribute to a broader understanding of non-seismic SSDS formation in nearshore settings and offer a valuable reference for similar features in formerly glaciated regions.

1. Introduction

Liquefaction is a process in which water-saturated sediments temporarily lose their shear strength, behaving as a plastic mass (cf. Casagrande, 1976; Obermeier, 1996; Maltman and Bolton, 2003; Owen and Moretti, 2011; Van Loon et al., 2020). This phenomenon typically results from increased pore pressure, which disrupts intergranular contacts and reduces sediment cohesion (Seed, 1979; Allen, 1982). Fine-grained sediments such as sandy silts and silty sands are particularly susceptible to liquefaction (Obermeier, 1996; Vanneste et al., 1999; Owen, 2003). Lacustrine and marine environments, consisting of

fine-grained sediments of varying density, are especially susceptible to liquefaction because of their water-saturated nature which contributes to instability (Allen, 1982; Reicherter et al., 2009; Van Loon, 2009; Van Loon et al., 2016; Pisarska-Jamroży and Woźniak, 2019; Belzyt et al., 2021; Pisarska-Jamroży et al., 2024).

Fluidisation also plays a key role in deformation and sediment mobilisation. Sediment mobilisation induced by liquefaction (Youd, 1973; Allen, 1982; Obermeier, 1996; Vanneste et al., 1999; Owen and Moretti, 2011) leads to the development of different SSDS (e.g., Jones and Omoto, 2000; Owen and Moretti, 2011; Yang et al., 2016; Woźniak et al., 2021; Pisarska-Jamroży et al., 2019a, 2022; Świątek and

* Corresponding author.

E-mail address: szymon.swiatek@amu.edu.pl (S. Świątek).

(Pisarska-Jamrozy, 2025). Water saturation plays a crucial role in the liquefaction process, as pore water facilitates pressure build-up under external forces, reducing effective stress and enabling sediment grains to move freely (cf. Allen, 1982; Seed et al., 1983; Phillips et al., 2018). This elevated pore pressure, often induced by rapid loading or shaking, serves as a precursor to sediment failure (Allen, 1982; Świątek and Pisarska-Jamrozy, 2025). Liquefaction generally occurs at shallow depths, where high pore pressures develop due to minimal overburden weight (Obermeier, 1996; Davies et al., 2004; Belzty et al., 2021; Świątek et al., 2023). Traces of liquefaction have been recorded to 10 m, though most are within the upper 2 m (Obermeier, 1996; Davies et al., 2004; Huang and Yu, 2013; Bronikowska et al., 2021). Near-surface sediments are more prone to mobilization and plastic deformation (Maltman and Bolton, 2003). With depth, the critical deformation state increases, reducing susceptibility. Liquefaction requires water saturation, overpressure, or insufficient compaction (Allen, 1982; Owen, 2003). Tang et al. (2016) suggested it occurs when relative density between layers is below 50 %, but it has also been observed at 58–92 % (Nakai, 2005) and 80 % (Wahyudi et al., 2013).

A variety of natural phenomena can trigger liquefaction. Seismic events are a major factor that generates sufficient stress to destabilise sediments (e.g., Sims, 1975; Alsop and Marco, 2011; Gibert et al., 2011; Phillips et al., 2018; Świątek et al., 2023). Rapid loading events, such as ice-sheet or glacier advances, iceberg calving, or sudden sediment deposition, can also induce liquefaction (Allen, 1982). Tectonic and glaciotectonic processes, as well as glacial isostatic adjustments (GIA), frequently provide the necessary stress to liquefy sediments, particularly in glaciogenic environments (Johnston, 1987; Muir-Wood, 2000; Stewart et al., 2000; Grollimund and Zoback, 2000; Van Vliet-Lanoë et al., 2004; Brandes et al., 2012, 2015, 2018, 2022; Hoffmann and Reicherter, 2011; Van Loon and Pisarska-Jamrozy, 2014; Pisarska-Jamrozy et al., 2018, 2019a, 2019b, 2022; Woźniak et al., 2021). Other external factors, such as tsunamis, storms, or meteorite impacts, can impose sudden and uneven pressure on sediment layers, further increasing liquefaction potential (Allen, 1982; Obermeier, 1996; Owen and Moretti, 2011).

Sedimentary features indicative of liquefaction arise under specific conditions and include various soft-sediment deformation structures (SSDS). Load casts and pseudonodules form when less dense sediments sink into underlying, denser, liquefied sediments (Džułyński, 1965; Pisarska-Jamrozy et al., 2019a; Świątek et al., 2023). Flame structures and ball-and-pillow features result from density instabilities and sediment displacement, reflecting liquefaction-induced deformation (Van Loon et al., 2020; Pisarska-Jamrozy et al., 2024). Water-escape structures, such as clastic dikes or sand volcanoes, indicate fluidisation by marking the expulsion of pressurised pore water (Belzty et al., 2021; Pisarska-Jamrozy et al., 2024; Świątek and Pisarska-Jamrozy, 2025). These deformation features provide critical insights into the triggers and conditions of past liquefaction events.

Morphological ambiguity among structures further complicates identification, as identical features of load casts, pseudonodules, and flame structures can develop under various conditions (Owen and Moretti, 2011; Moretti and Van Loon, 2014). Distinguishing between deformation caused by seismic activity and that resulting from over-loading, mass movements or cryoturbation is often challenging (cf. Van Vliet-Lanoë et al., 2004; Horváth et al., 2005; Pisarska-Jamrozy and Woźniak, 2019; Van Loon et al., 2020; Woźniak et al., 2021).

Given these challenges, it is essential to integrate multiple lines of evidence, including sedimentological, structural, and stratigraphic analyses, to infer liquefaction triggers accurately (McCalpin et al., 2023). Advanced modelling (Bronikowska et al., 2021) and detailed field investigations are crucial for improving our understanding of deformation structures in the sedimentary record. This issue is particularly significant in transitional environments between land and sea, where high water content, heterolithic sediment composition, and fluctuating depositional conditions enhance sediment susceptibility to liquefaction. Identifying a

single triggering mechanism in such settings is challenging, as multiple factors often interact. The Sārnate site, investigated in detail in this study, hosts a diverse and complex suite of deformation structures that offer a valuable basis for examining liquefaction processes, potential triggers, and environmental controls in a transitional coastal environment.

The primary aim of this study is to enhance our better understanding of sediment liquefaction processes in nearshore environments. The specific objectives are to: (1) characterise liquefaction-related sedimentary features through linking deformation structures with specific rheological properties of the sediments; (2) assess environmental and geological factors influencing liquefaction susceptibility, focusing on grain size, sedimentary setting, and water saturation; (3) identify trigger mechanisms, particularly the roles of pore water pressure and external forces; (4) apply sedimentary evidence to reconstruct past liquefaction events and evaluate their geological significance.

2. Geological setting

The Sārnate study site ($57^{\circ}04'01.34''\text{N}$, $21^{\circ}24'55.88''\text{E}$) is located in the Ventava Plain of the Piejūra Lowland in western Latvia, approximately 37 km S/SW of the town of Ventspils (Figs. 1A and 2). The outcrop is situated in the southern section of a 3 km long stretch of an ancient Littorina Sea lagoon (Ventspils lagoon), which has been extensively eroded by modern coastal processes (Fig. 1A).

One main geological-tectonic structure called the Liepāja-Rīga-Pskov Fault Zone (LRPFZ) of early Palaeozoic age, has been distinguished in the proximity of the study area (Stolarczyk, 1979; Brangulis and Kanev, 2002; Tuuling, 2019). The LRPFZ (Fig. 1B), formed as a result of the Baltica-Avalonia-Laurentia collision, divides Latvia into two zones: the southern zone (with faults up to 200 km long and a throw of up to 200 m) and the northern zone (with faults up to 60 km long and a throw of up to 20 m; Misans and Brangulis, 1979; Paškevičius, 1997; Modliński et al., 1999; Tuuling, 2019). The crystalline basement near the Sārnate site lies at a depth of approximately 1200 m. The sedimentary cover of Latvia comprises four structural complexes, separated by unconformities (Fig. 1C and D; Siveizdis et al., 1979; Šliaupa and Hoth, 2011): the Baikalian complex (late Neoproterozoic terrestrial and marine sediments up to 30 m thick), the Caledonian complex (Cambrian to Lower Devonian deposits up to 1000–1200 m thick), the Variscan complex (Middle Devonian carbonate rocks up to 50 m thick, directly overlain by Quaternary sediments), and the Alpine complex (in western Latvia, only up to 200 m thick Quaternary deposits linked to Pleistocene glacial and interglacial processes occur). Above the Middle Devonian bedrock lies Saalian till (MIS 6; Fig. 1D), overlain by the Akmenrags Formation (Fig. 1D). The Early Weichselian Jūrkalne 1 and 2 formations (Fig. 1D), locally overlain Middle Weichselian glaciofluvial deposits and thin glacial till lenses. More commonly, Jūrkalne 2 is overlain by Jūrkalne 3 Formation, capped by a 2–3 m Late Weichselian till (Fig. 1D). The Jūrkalne 3 Formation was partially eroded during the Baltic Ice Lake (BIL) stage (Grinbergs, 1957). The area became ice-free after the retreat of the Valdemārpils ice-marginal zone around 14 ka (Saks et al., 2007, 2011; Zelčs et al., 2011; Zelčs and Nartišs, 2014). Following deglaciation, the region was submerged under several stages of the BIL development with water depths at the site exceeding 20 m (Fig. 2). During the Yoldia Sea stage the site was located above its water level (Veinbergs, 1979). The shoreline of Ancylus Lake is no longer discernible in this area (Breijers et al., 2023), as it is assumed to be eroded during later stages of the Littorina Sea (Grinbergs, 1957). Analysis of plant macroremains and pollen indicates dry or near-dry land conditions after inundation by the short lived Ancylus Lake (Kalinija et al., 2019). A water level drop of at least 10 m between Ancylus Lake maximum and onset of Littorina Sea has also been observed on the eastern side of Kurzeme peninsula, at former Littorina Sea lagoon in Gipka (Rosentau et al., 2023), a region with similar uplift as Ventspils lagoon (Grinbergs, 1957). During the Littorina Sea maximum, the shoreline (Grinbergs, 1957) was situated

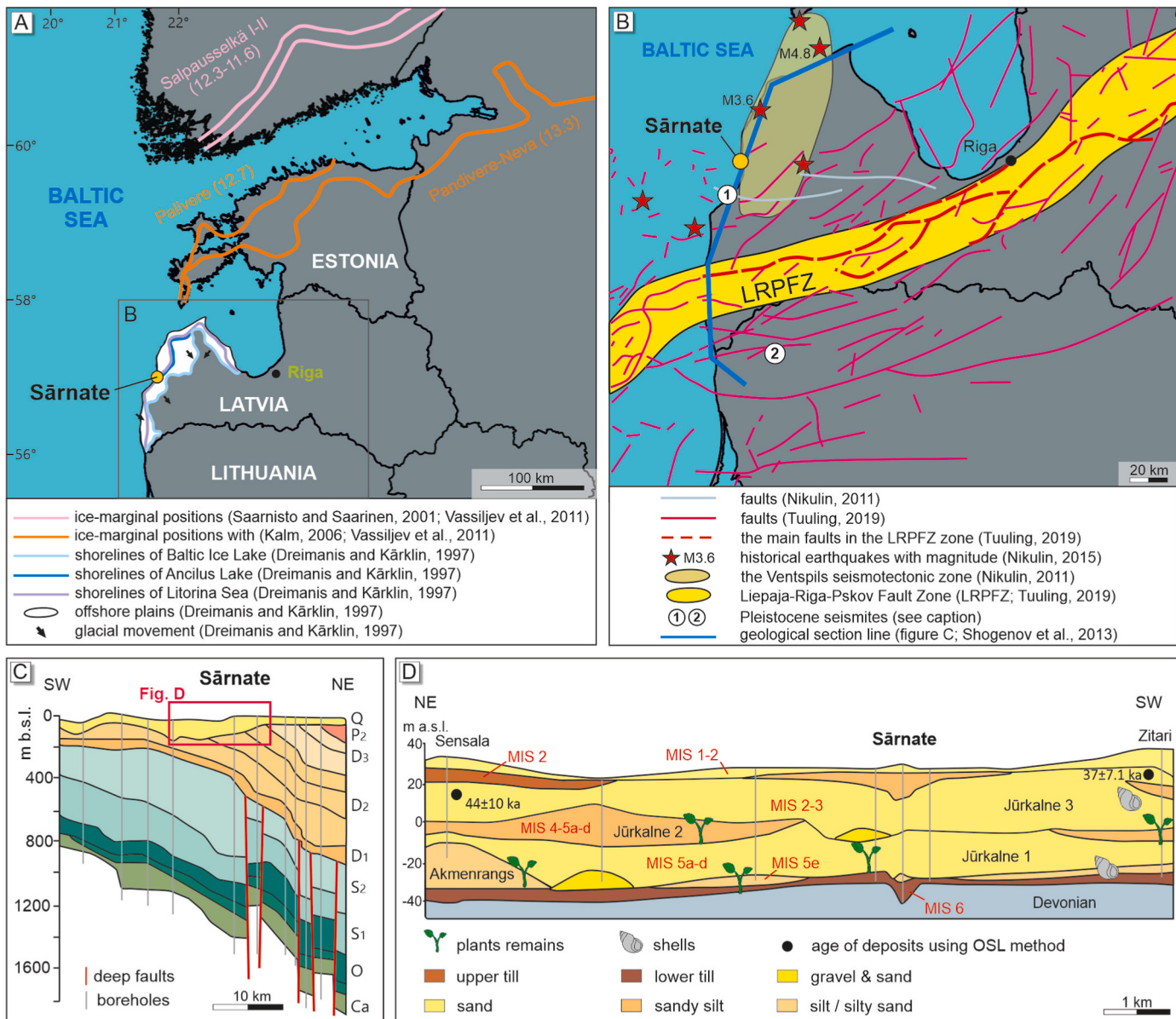


Fig. 1. Location of the Särnate study site. (A) Ice-marginal positions with ages (cal ka) and extent of the Baltic Sea phases (Saarnisto and Saarninen, 2001; Vassiljev et al., 2011; Dreimanis and Kärklin, 1997). (B) Seismotectonic map (Nikulin, 2011; Tuuling, 2019) sites with SSDS interpreted as seismites: 1 – Baltmuiza site; Woźniak et al. (2021), 2 – Dyburiai site; Belzyt et al. (2021). (C) Synthetic geological cross section across Latvia (for locations of boreholes see Shogenova et al., 2009; Shogenov et al., 2013; Ca - Cambrian, O - Ordovician, S₁ - Lower Silurian, S₂ - Middle Silurian, D₁ - Lower Devonian, D₂ - Middle Devonian, D₃ - Upper Devonian, P₂ - Upper Permian, Q - Quaternary). (D) Simplified geological cross section (Saks et al., 2012; Woźniak et al., 2021, modified).

approximately 600 m southeast of the site (Fig. 2). At that time, the area was part of a bay that eventually became completely isolated from the open sea due to a relative drop in sea level caused by GIA of the Earth's crust (Saulite et al., 2007; Kalniņa et al., 2019). Radiocarbon dating of lagoonal organic material in the vicinity of Särnate site has yielded calibrated ages of 3450–3560, 5990–6130, and 7580–7730 years BP from the top to the bottom of the sequence (Saulite et al., 2007). The region subsequently underwent postglacial uplift, resulting in its current position on an erosional surface approximately 10 m above present sea level. The isostatic uplift rates range between 3 and 4 mm/year (Tikkannen and Oksanen, 2002; Zelčs and Nartišs, 2014) and ~0.8 mm/year (Varna et al., 2019).

In this region, liquefaction-induced SSDS have already been identified. At the Baltmuiza study site, located 25 km southwest of the Särnate site (Fig. 1B), seismically-induced SSDS within shallow marine bay silty-sandy sediments were documented by Woźniak et al. (2021). These

deformations are interpreted as having been triggered by mid-Late Weichselian icequakes at the front of the advancing Fennoscandian Ice Sheet (FIS), with deformation estimated to have occurred between 30.5 ± 1.8 ka and 26.3 ± 1.5 ka OSL (Woźniak et al., 2021).

3. Methods

The sedimentary succession at the Särnate site was logged along the outcropping section, which is 2.9 m high (0.4 m–3.3 m above present sea level) and 20 m wide (fieldwork was carried out in June and September 2018). Fieldwork was conducted along a longer stretch of the coastline. However, no similar sedimentary succession was identified. The sedimentary profile was divided into two units (A and B) based on stratigraphy and sedimentary properties, within which several trough-shaped structures were distinguished (Fig. 3). The textural and structural characteristics of the sediments were described using the lithofacies

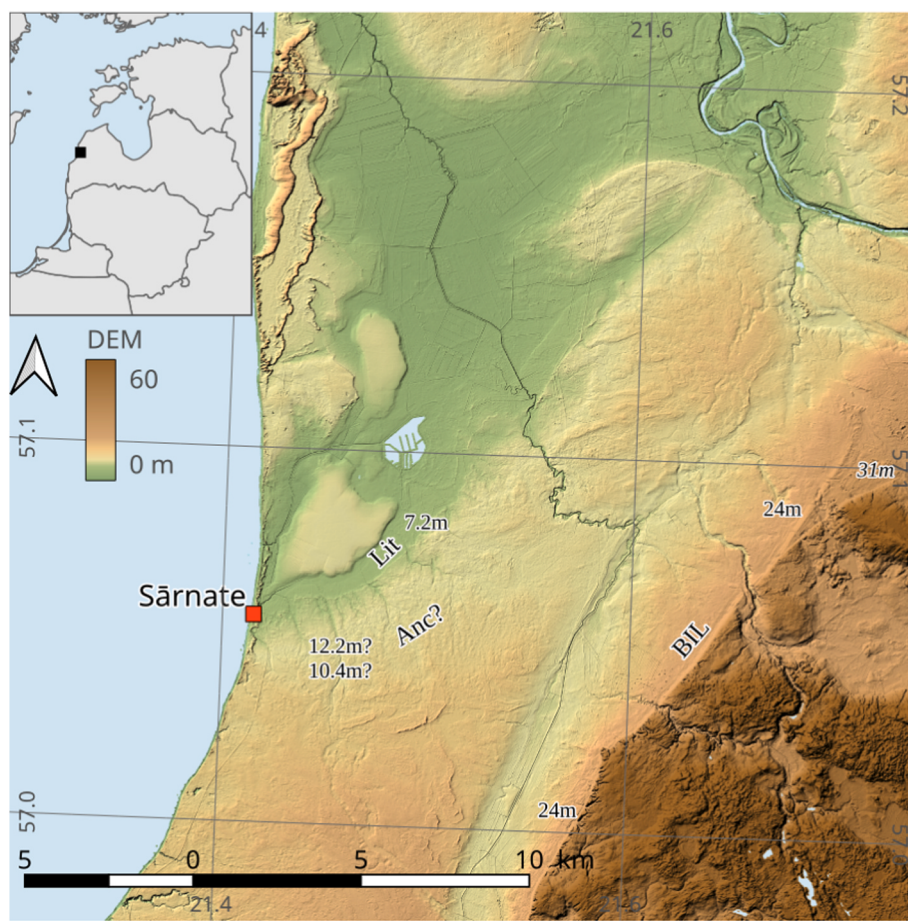


Fig. 2. LiDAR topography of the study area and position of the Särnate site relative to the shorelines of the Baltic Ice lake (BIL), the Littorina sea (Lit) and the potential Ancylus lake shoreline (Anc). Numbers indicate approximate elevations at the base of erosional scarps, thus marking minimal water level. The colour scale indicates present-day elevation (metres above sea level) based on the digital elevation model (DEM). (For interpretation of the references to colour in this figure legend, the reader is referred to the Web version of this article.)

approach initially presented by Miall (1977) and modified by Zieliński and Pisarska-Jamrozy (2012). The most commonly occurring lithofacies in these units were grouped into lithofacies associations, in which the order of lithofacies reflects their abundance within the sedimentary succession, with the most widespread listed first. Based on these lithofacies associations, hydrodynamic reconstructions of the environmental conditions were carried out.

Twenty-three samples were collected from lithofacies for grain size analysis. Grain size distribution was determined by the laser diffractometry method using Maltman and Bolton, 2003 (with Hydro, 2000G analyser), processed with GRADISTAT 8.0 software, and presented on the Friedman and Sanders, (1978). Basic grain size statistical parameters proposed by Folk and Ward (1957) were used for data analysis.

Two samples (Fig. 3B; sample GdTL-3200 and sample GdTL-3201) from the lower part of unit A were collected for optically stimulated luminescence (OSL) dating using 30-cm long opaque tubes to prevent sunlight exposure. These samples were taken from undeformed layers that underlie the described layers with SSDS and were dated at the GADAM Gliwice Luminescence Laboratory using the standard multi-grain aliquots method on coarse-grained quartz (90–125 µm). To estimate the age of the deposits, the minimum age model (MAM) was applied (Fig. 4), as the subaqueous depositional environment provided insufficient sunlight exposure for complete signal resetting. This limited exposure can cause the luminescence age to fall between the deposit's true age and the age of its parent sediment, often resulting in an overestimated age (see Pisarska-Jamrozy et al., 2022).

Due to the abundance and extremely diverse range of sedimentary

structures observed at the Särnate site, the description and interpretation were conducted at both the mesoscale, covering the entire exposure, and at the microscale in selected areas, specifically those with distinctive depositional, erosional, and deformation structures or key boundary zones, such as sedimentary lithofacies contacts. Four undisturbed samples for thin section analysis were collected from the selected parts of the Särnate sedimentary profile (thin section samples TS1, TS2, TS3, TS4 ordered from the bottommost part to the uppermost; for location see Fig. 3A). Sample TS1 was collected from the lowermost part of a trough-shaped structure eroded within the horizontally-laminated sands of unit A and contains silty clasts infilling the bottom parts of the trough (see Fig. 3). Sample TS2 was collected from the erosional contact zone between the uppermost part of unit A and a trough-shaped structure with a sand-dominated infilling, located between units A and B (see Fig. 3). Sample TS3 represents the infilling of the bottom part of a trough-shaped structure between units A and B (see Fig. 3). Sample TS4 represents the contact between an injection structure and overlying horizontally-laminated, sand-dominated sediments of unit B (see Fig. 3). Samples were collected and prepared following the methodology described by Menzies and van der Meer (2018). Thin sections (6 × 9 cm) were analysed using a Nikon Eclipse LV100 polarisation microscope (plane-polarised light) with a motorised XY stage and camera, supplemented by high-resolution scans from an Epson V37 device. Microstructural interpretation and mapping were performed using CorelDRAW software, with a focus on grain characteristics, sedimentary structures, and key structural discontinuities to reconstruct the deposition, followed by erosion and deformation sequence (e.g., Phillips et al., 2011; van der

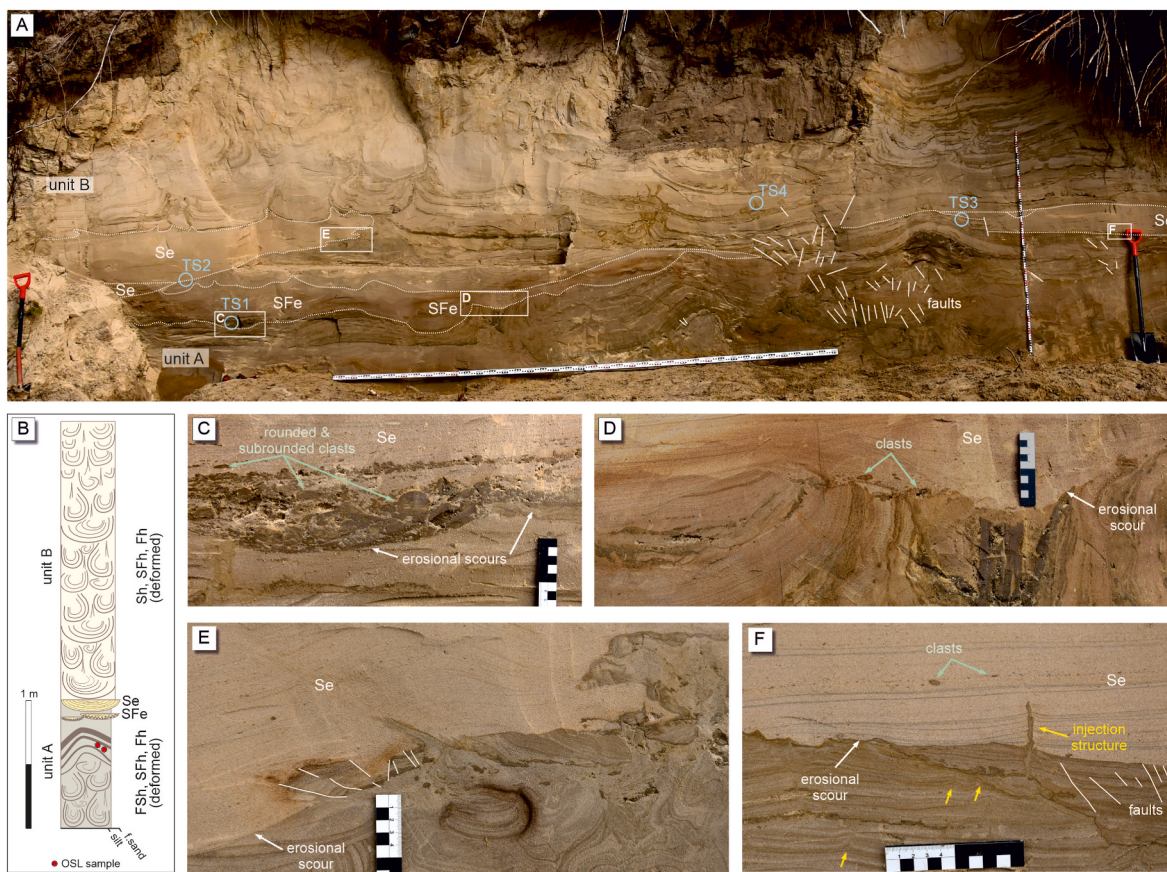


Fig. 3. General view of the Särnate site. (A) Location of units A (lithofacies association of horizontally-laminated sandy silts, silty sands and silts: FSh, SFh, Fh) and B (lithofacies association of horizontally-laminated sands, silty sands and silts: Sh, SFh, Fh), as well as troughs with an erosional scours (lithofacies of sands and silty sands with erosional scours fill: Se and SFe); location of sampling sites for undisturbed structure samples TS1-TS4 (blue circles) and faults (white solid lines). (B) Schematic sedimentary log. (C-F) Erosional scours at the base of troughs and rounded/subrounded silty clasts in the lower part of troughs (C, D), injection structures (E, F) and faults (F). (For interpretation of the references to colour in this figure legend, the reader is referred to the Web version of this article.)

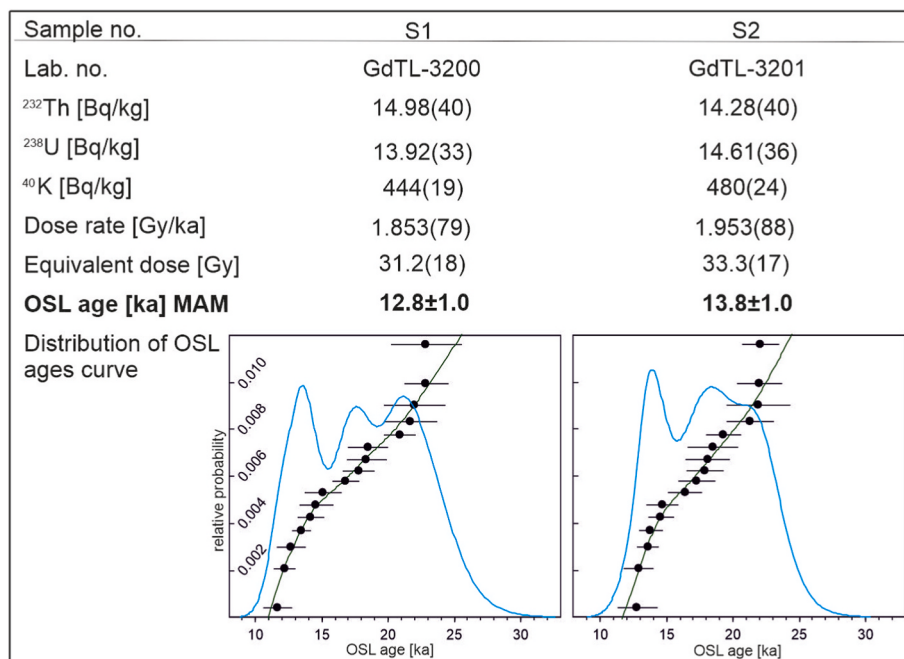


Fig. 4. OSL dating results for the lower unit A, with ages (bolded) based on the minimum age model (MAM).

(Meer and Menzies, 2011). A complete description of the thin section samples is provided in [Supplementary Material 1](#). Additionally, selected parts of thin sections were analysed using a Scanning Electron Microscope (SEM) at the University of Warsaw (Poland) to examine the morphology and fracturing of quartz grains. The analysis also aimed to detect potential gold accumulations within the liquefied sediments, associated with the seismic origin hypothesis, following the method proposed by Świątek et al. (2025).

4. Results

4.1. Sedimentary succession

The sedimentary succession at the Särnate site was observed in a 2.9 m high and 20 m wide exposure, oriented NE-SW ([Fig. 3A](#)), along the Latvian Baltic Sea coast. It comprises two main lithofacies associations: a lower lithofacies association FSh, SFh, Fh designated as units A, and an upper lithofacies association Sh, SFh, Fh designated as unit B ([Fig. 3B](#)). Above unit B, a 0.5 m thick layer of soil is present. In the central part of the outcrop, a cuboid-shaped depression of anthropogenic origin is filled with mixed sediments and soil. The surface morphology above the outcrop has also been altered by human activity ([Fig. 3A](#)). SSDS within units A and B were documented exclusively in the studied outcrop. Equivalent successions with similar deformation structures are lacking in exposures along the coastline to both the north and south, highlighting the distinctive character of the Särnate site. SSDS, which commonly occur within the sedimentary succession at the Särnate site, are described in detail in section [4.2](#).

The OSL dating results indicate MAM ages for the lower part of unit A ([Fig. 4](#)), ranging from 13.8 ± 1.0 ka to 12.8 ± 1.0 ka. There are no Holocene lagoonal deposits at the Särnate site, whereas they can be traced for at least a few hundreds of meters along the coast to the north of the site and have been described by Saulite et al. (2007), which is reported to have been deposited during the Litorina Sea stage.

4.1.1. Description

Unit A has a minimum thickness of approximately 1.05 m (its lower boundary was not excavated) and primarily consists of rhythmically occurring sandy silts and silty sands ([Fig. 3A](#) and [5](#)). The upper boundary of unit A is sharply defined but irregular in shape. This unit contains

horizontally-laminated sandy silts, silty sands, and silts (lithofacies association FSh, SFh, Fh), with thicknesses ranging from a few centimetres to 10 cm. These sediments are interbedded with individual thin horizontally-laminated silty laminae (lithofacies Fh), ranging in thickness from a few millimetres to 2 cm. The clay fraction content does not exceed 5 % in any of the analysed samples ([Fig. 5](#)).

The upper unit B, approximately 1.85 m thick, consists of rhythmically occurring horizontally-laminated fine-to very fine-grained sands, silty sands and silts (lithofacies association Sh, SFh, Fh; [Fig. 3A](#) and [5](#)). The rhythmic sequences reach up to ~40 cm in thickness, with coarser sandy sediments forming the lower part of the rhythm and finer silty sands in the upper part. The thickness of individual lithofacies ranges from 1 to 20 cm. The lithofacies Sh, SFh are interbedded with thin laminae of horizontally-laminated silts (lithofacies Fh) measuring 1–2 cm thick.

Between units A and B, a few trough-shaped structures occur at almost the same hypsometric levels within the uppermost part of unit A ([Fig. 3C–F](#)). The smaller ones measure 7–14 cm in height and 20–80 cm in width, while the largest reach a height of 22–45 cm and a width of 135–200 cm. The lower boundaries of these troughs are sharply defined, sometimes exhibiting an irregular shape (in details described in section [4.2](#)). The troughs are filled with laminated silty sands and fine-grained sands (lithofacies SFe, and Se, respectively), with the laminae conforming to the trough shape. Locally, the internal structure of this infill is strongly disrupted, as seen in the microscale image of thin section sample TS3 ([Fig. 6A–A'](#); for location, see [Fig. 3](#)).

In the lower parts of the troughs, silty clasts ([Fig. 5](#)) ranging from subrounded to rounded in shape and measuring in mesoscale between 0.5 and 2 cm in diameter, were identified ([Fig. 3C–F](#)). One example of such fine-grained infill in the bottom parts of a trough is presented in detail in thin section sample TS1, which represents the lowermost part of a trough-shaped structure cut into the horizontally-laminated sands of unit A ([Fig. 6B–B'](#); for location, see [Fig. 3](#)). In the central part of the thin section sample TS1, 200 chaotically arranged silty clasts were counted. These clasts exhibit irregular shapes, ranging from spherical and ellipsoidal to elongated, and vary in size, with diameters ranging from 0.1 mm to a few centimetres. Additionally, they display strongly disrupted and folded internal lamination, with chaotically-oriented fold axes.

The analysed quartz grains from thin sections, including units A and B, as well as sediments from erosional scours at the base of troughs,

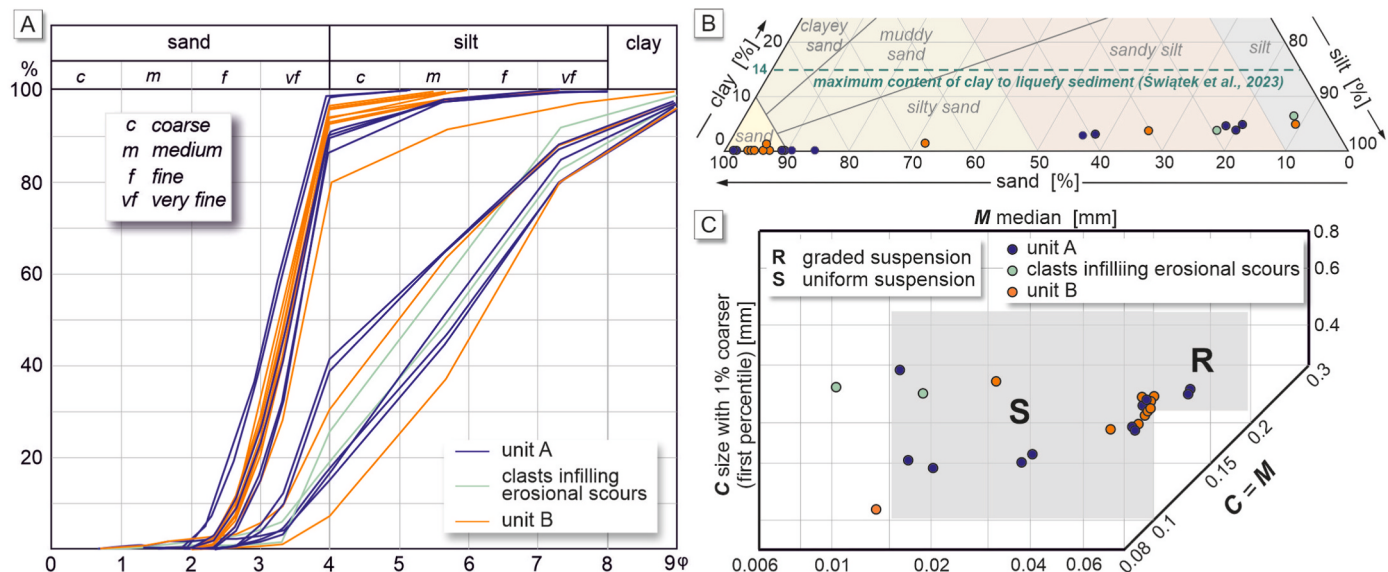


Fig. 5. Overview of textural features of liquefied sediments at the Särnate study site. (A) Grain-size cumulative curves. (B) Triangle diagram of grain-size (after Friedman and Sanders, 1978) and sediment classification (after Folk, 1954). Note that the clay fraction does not exceed 5 % in any of the analysed samples. (C) Distribution of liquefied sediment samples on the C/M diagram (after Passegård, 1964; Passegård and Byramjee, 1969).

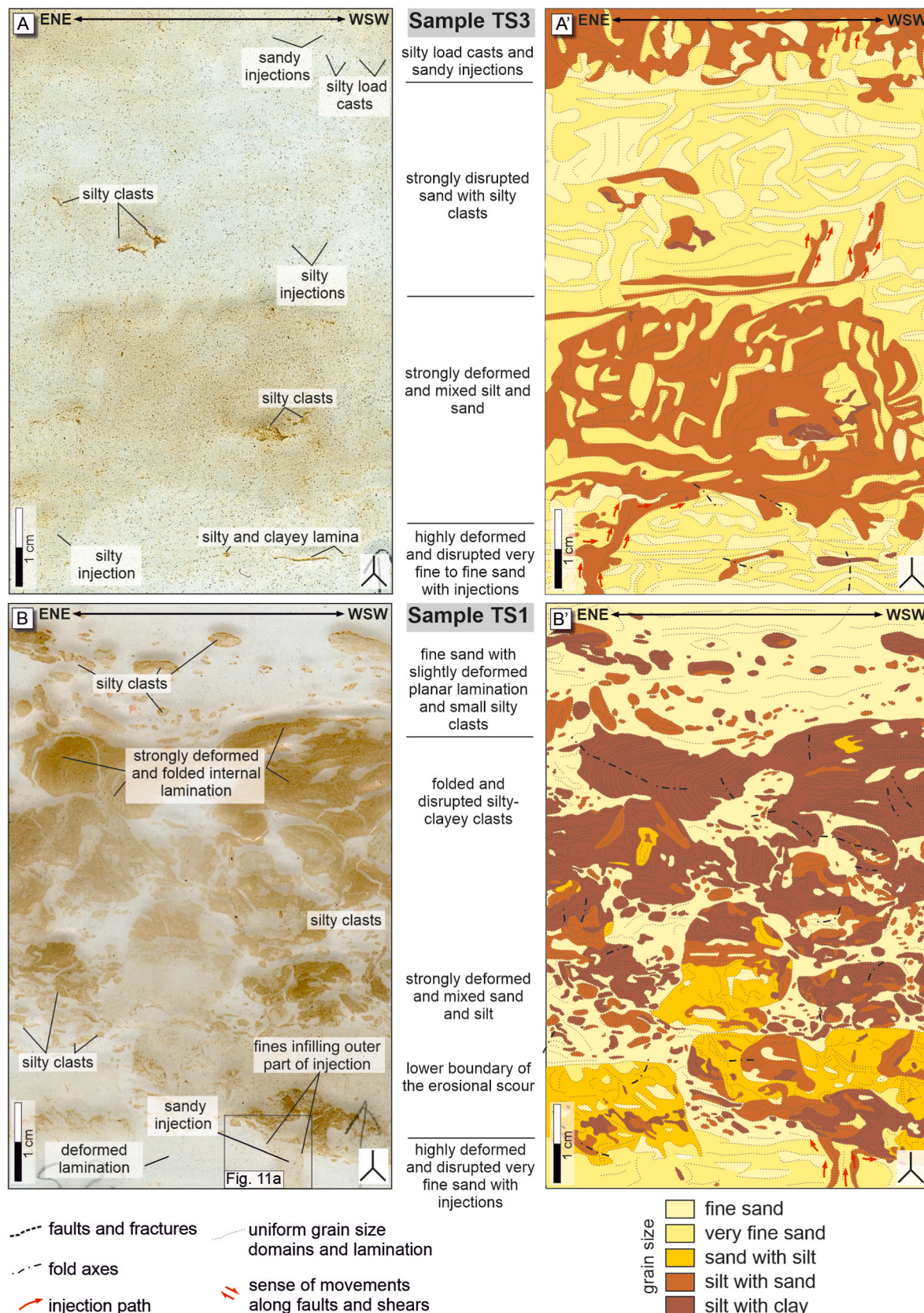


Fig. 6. High-resolution scans of the thin sections and interpretation of the microsedimentology within two samples from the Särnate study site: (A) and (A') sample TS3, which represents the infilling of the bottom part of a trough-shaped structure between units A and B (see Fig. 3); (B) and (B') sample TS1, that was collected from the lowermost part of a trough-shaped scour eroded within the horizontally-laminated sands of unit A and contains silty clasts infilling the bottom parts of the trough (see Fig. 3A–C).

exhibited diverse morphologies ranging from rounded to irregular and angular shapes (Fig. 7). Some grains displayed distinct features such as microdepressions (Fig. 7), while no quartz damage in the form of inclusions were observed.

No significant quartz fracturing was identified, either in the form of cracks or larger-scale fracturing. Only a few grains exhibited minor cracks, but these were not well-developed (Fig. 7). In addition to quartz grains, a substantial presence of heavy minerals was observed, particularly zircon and ilmenite (Fig. 7). Apart from visible differences in the size of sediment components, no evidence indicating the direction of liquefaction was observed.

4.1.2. Interpretation

Sediments in unit A were deposited mainly from uniform suspension, with some contribution from graded suspension (Fig. 5C), under very calm conditions typically associated with subaqueous environments (Smith and Ashley, 1985; Brodzikowski and Van Loon, 1991; Best et al., 2005; Gilbert et al., 2006; Pisarska-Jamrozy, 2013). The rhythmic occurrence of horizontally-laminated sediments of lithofacies FSh, SFh, Fh (unit A) indicate rhythmical changes in the depositional environment (Ashley, 1975) most likely linked to the seasonal variations in the sedimentary environment (see details in section 6).

Horizontally-laminated sands and silty sands (lithofacies Sh, SFh) of unit B were deposited from mainly graded suspension (Fig. 5C). The individual silty laminae (lithofacies Fh) were deposited from uniform suspension. Unit B, like unit A, was deposited under subaqueous conditions. However, the slightly coarser grain size of the sediments in unit B, compared to those in unit A, suggests shallower conditions where storm and wave action actively influenced deposition. Sandy troughs (Fig. 3C–F), occurring in the Särnate sedimentary succession, with sharply-defined lower boundaries, suggest an origin from erosional scours at the base of troughs (cf. Miall, 1985). The occurrence of silty clasts in the lower part of the troughs can be explained by the erosion of underlying silty sediments by waves and currents, involving two main processes: (1) detachment and incorporation of eroded lower-lying sediment from unit A, followed by (2) rotation of silty clasts, accompanied by rolling and folding of elongated clasts due to pressure changes generated during the energetic channelized flow. The surrounded and

rounded clasts, exhibiting spherical, ellipsoidal, and elongated shapes, suggest that they were either rounded relatively quickly due to wave action and current activity or transported by currents (cf. Pisarska-Jamrozy and Zieliński, 2012). Such silty clasts can be interpreted as rip-up clasts (cf. Allen, 1982, 1987), which commonly occur on wave-dominated coasts (cf. Leckie, 1988; Bández et al., 2018; Kongsen et al., 2021). The currents that led to the development of erosional scours at the base of troughs were not catastrophic, as their infill is characterised by laminae conforming to the trough shape (lithofacies SFe, Se). The occurrence of erosional scours at the base of troughs at approximately the same elevations suggests that these events occurred at the same time in the Särnate sedimentary succession.

4.2. Deformation features

4.2.1. Description

The Särnate outcrop features a wide range of mesoscale and microscale deformation structures, including (1) folds, (2) faults and fractures, (3) hydrofractures, (4) fragments of broken-up laminae, (5) load structures and flame structures, and (7) injection structures (Fig. 8).

- (1) The unit A is undulating, forming both synforms and antiforms (Fig. 3A), which do not occur in the upper unit B. Most of the folds are upright, symmetrical, and gentle, with interlimb angles ranging from 155° to 160°. Steeply inclined folds, occurring in the central and western parts of the outcrop, exhibit interlimb angles of 95°–135° (Fig. 9A–C). In the uppermost parts of these antiforms, discontinuous laminae (=deformed fragments of broken-up laminae described in detail below) are observed. Folds are also present in all samples (TS1–TS4) analysed at the microscale (Figs. 6 and 10). They exhibit diverse geometries, vary in size, develop in sediments with varying textures, and have irregularly oriented fold axes (Figs. 6 and 10); some are associated with injection structures (Fig. 6A–A' and Fig. 10). Slight folding also affected the erosional scours at the base of troughs occurring in unit A (Fig. 3D–F).
- (2) Small-scale, steeply inclined normal faults and fractures (Fig. 3A), with dips ranging from 60° to 85°, occur primarily in

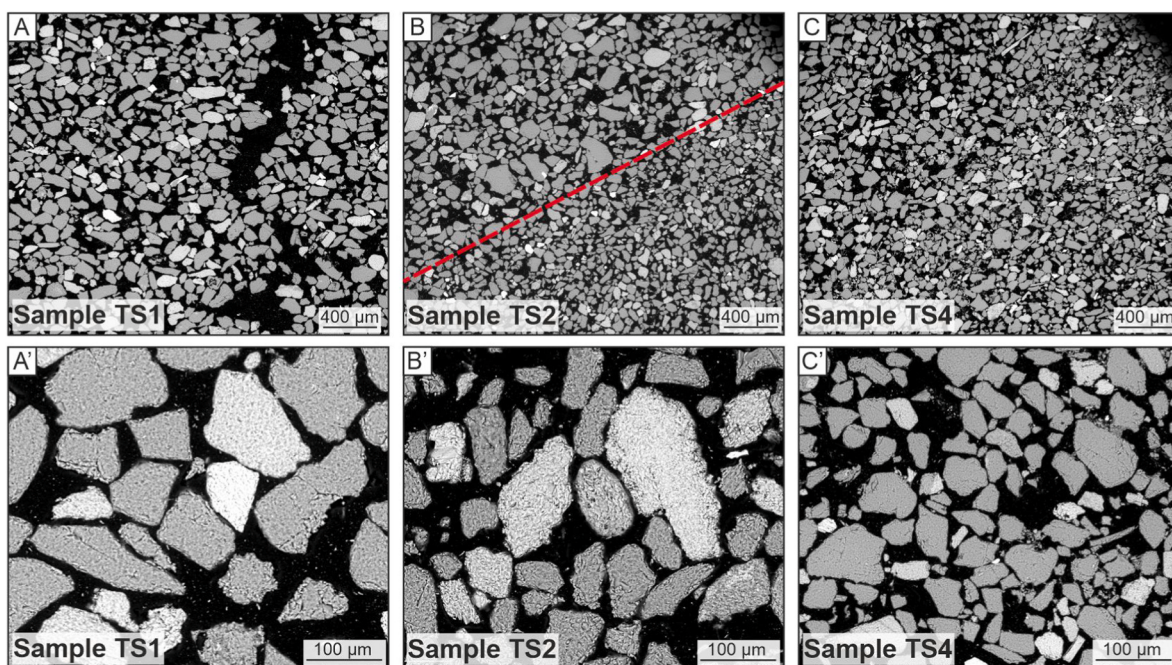


Fig. 7. Morphology of quartz grains based on SEM analysis of the selected parts of thin sections. Red dashed line indicates the erosional boundary. (For interpretation of the references to colour in this figure legend, the reader is referred to the Web version of this article.)

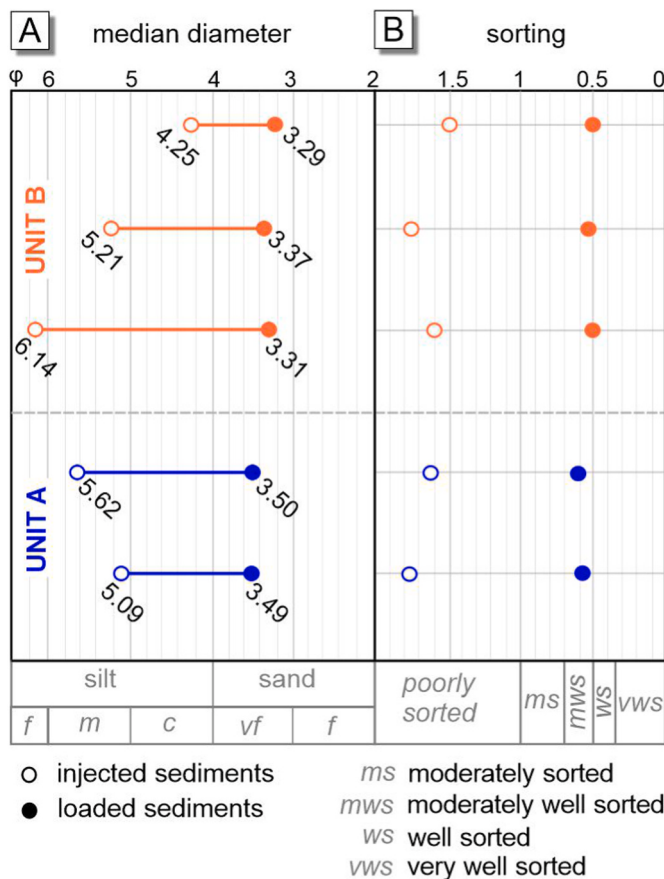


Fig. 8. Selected textural parameters of soft-sediment deformation structures: comparison of loaded and injected sediments. (A) Median grain diameters of injected and loaded sediments. (B) Distribution of sorting parameter in injected and loaded sediments.

unit A, beneath the erosional scours at the base of troughs (Fig. 3E and F) and, as smaller, secondary features, within antiforms (Fig. 9C). Offsets of mesoscale faults range from a few millimetres to 7 cm maximum. At the microscale, a single fault was exclusively identified in thin section sample TS4 representing the contact between a mesoscale injection structure and the overlying horizontally-laminated sands of unit B (Fig. 10A–A'; for location, see Fig. 3). This small-scale normal fault is located at the boundary between two grain-size domains (silt with sand and very fine-grained sand), which aligns with the outer margin of the main injection structure observed in the thin section sample TS4 and has an offset of 0.2 cm (see the lower-central part of Fig. 10A–A').

- (3) Hydrofractures are recognised only in unit B. They are oriented vertically and semi-vertically (Fig. 11C). Their height ranges from 3 to 20 cm, and their width is 2–4 cm. Hydrofractures are infilled with sandy silts and silty sands, as well as millimetre-sized rounded and subrounded silty clasts (Fig. 10B–B').
- (4) Fragments of broken-up laminae are rare and have been identified in unit B (Fig. 9A and 11C), as well as in the antiforms in unit A (Fig. 9B and C). These in unit B (Fig. 7C and 9A) are subangular in shape, with length of 6–15 cm and a height of 5 cm. The fragments contain a set of horizontally-laminated silty sands. Fragments of broken-up laminae in antiforms in unit A (Fig. 9B and C) are thin, measuring 1 cm in thickness and up to 20 cm in length. Their shape is angular, slightly undulating, and resembles a long beak.

(5) Load structures (load casts, pseudonodules) occur in groups in the lower part of unit A and are widespread in unit B (Fig. 9A and 11). The load casts in unit A (Fig. 9A) range from 10 to 15 cm in width and 7–12 cm in height, and are characterised by internal lamination parallel to their outer shape. In the upper part of unit B, load casts are larger, reaching up to 1.8 m in width and 0.8 m in height. Additionally, pseudonodules measuring 5 cm in width and 6 cm in height occur (Fig. 11B). The load structures are composed of predominantly well-sorted sandy sediments (Fig. 8). The internal lamination of most load casts in unit B is parallel to their outer shape (Fig. 11A). However, some exhibit horizontal lamination that is not linked to the outer shape (Fig. 11C). Microscale observations confirm the presence of load casts in thin section samples TS2 and TS3 (Fig. 6A–A' and 10B–B' Fig. 6). Within the main injection structures of TS2 and TS3, small-scale load casts occur (Fig. 9B and 10B'). In TS3, single pseudonodules are additionally present in the uppermost part of the sample, where they are closely associated with upward-directed, small-scale injections of sand (Fig. 6A–A').

Load casts are always accompanied by flame structures, which occur in the lower and western parts of unit A and are also widespread in unit B (Fig. 11). They are up to 15 cm in height and 1–3 cm in width. Flame structures, occurring between load casts, are silty, upwards-oriented structures (Fig. 11).

(6) Injection structures, oriented vertically and sub-vertically, are common in unit A (Fig. 3E–F and 9A,B,D,E), in unit B (Fig. 3A and 11B–C), and in the lower part of troughs (Fig. 2E–F). These structures propagate upwards and range in size from 4 to 20 cm in height and 0.5–3 cm in width. The largest structures are found in the lower part of unit A (Fig. 9D and E), reaching up to 20 cm in height and 1 cm in width, with the width gradually decreasing upwards. Injection structures are most abundant in unit B, where their morphology is also the most complex (Fig. 11B–D). Microscale observations show that some vertically-oriented, upward-tapering single injection structures contain silty sediments but may also have fine-grained sand at their core and sandy silt at the margins, all cutting through highly deformed and disrupted laminae of very fine-grained to fine-grained sand (thin section samples TS1–TS3; Figs. 6 and 12A). There are also injection structures which, in their lower part, contain mixed sediment, ranging from fine-grained sand to silt, with contorted lamination, while in the upper part, several downward-curving clasts of silty sand and silt are present, with finer (silt-rich) sediments concentrated at the margins (thin section sample TS4; Fig. 10B–B' and 12C). The injection structures are composed of poorly-sorted silty sediments (Fig. 8).

Certain SSDS occur more frequently in one unit than in the other, and their geometry varies depending on their position within the sedimentary succession (Fig. 3B). Furthermore, another relationship has been noted: injected structures are infilled with poorly sorted finer sediments, ranging from silty sands to fine-grained silts (silt content: 31–88%; clay content: 1.6–4.4%), whereas loaded structures are infilled with very fine-grained sands (sand content: 87–98%) that are moderately well-to well sorted and contain no clay (Fig. 8).

4.2.2. Interpretation

The difference in the deformation styles of the lower and upper units may be attributed to subtle variations in sediment rheology resulting from slight textural differences. Poorly sorted, finer sediments (ranging from fine-to coarse-grained silts) were more susceptible to injection, whereas moderately well-to well-sorted very fine sands were more prone to loading (Fig. 8; cf. Świątek et al., 2023). The sedimentary succession at the Sarnate site is composed entirely of liquefaction-prone sediments,

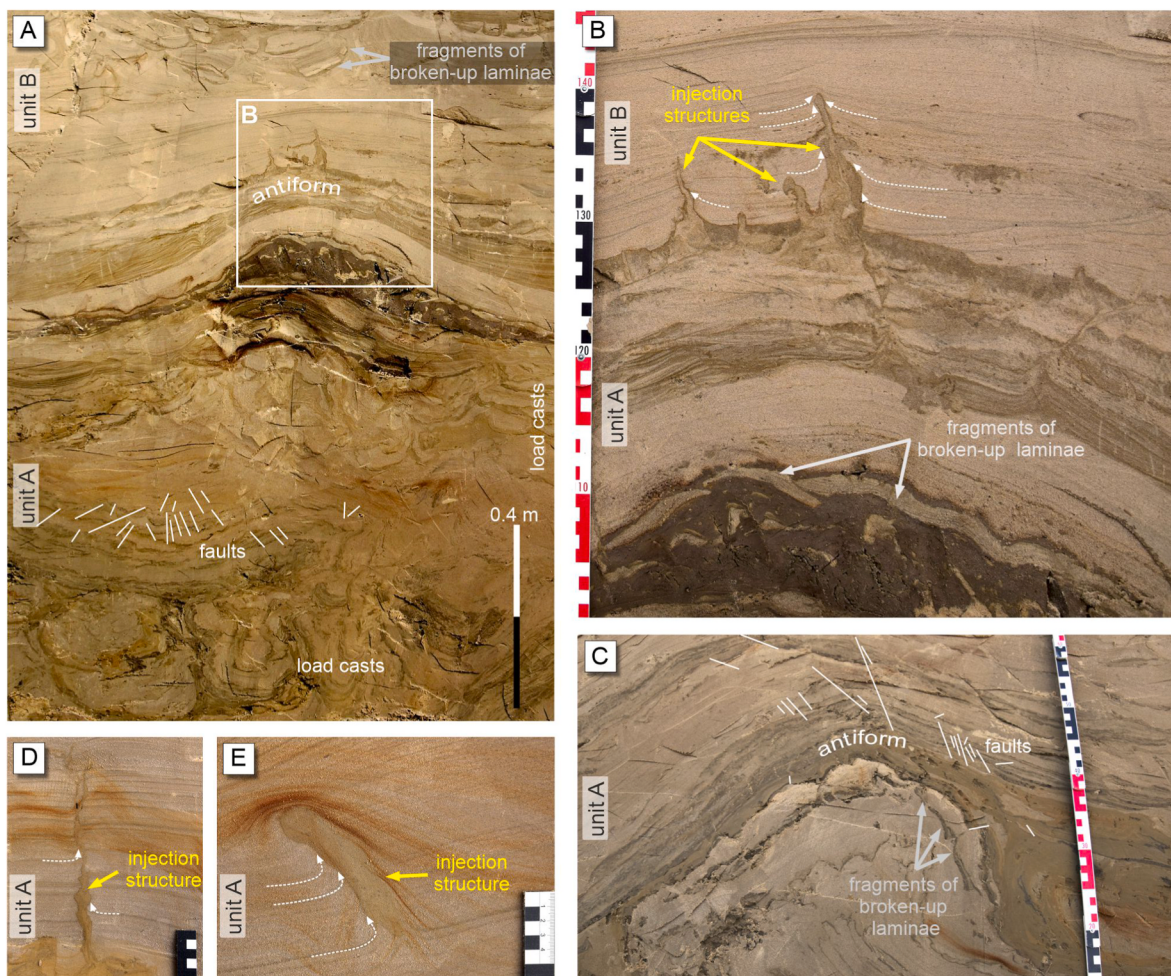


Fig. 9. Deformation structures in units A and B. (A–C) Antiforms with injection structures and faults surroundings. (D–E) Silty injection structures. Note the upward-curving laminae surrounding the injections (white dashed lines).

such as fine-grained sand and silt (cf. Obermeier, 1996, 2009; Świątek et al., 2023).

- (1) The undulating sediments in unit A, which display predominantly upright, gentle folds on a large scale and diverse geometries at the microscale, may have resulted from vertical pressure induced by uneven overloading caused by the weight of overlying sediments and water. As most fold axes are oriented parallel to the main injection axis (Fig. 9A–C and 10), we conclude that the folding may also have been induced by the upward intrusion of liquefied sediment, causing localised upward bending of sediment laminae, reminiscent of fold-like structures. The deformation occurring within the folds suggests high pore-water pressure during the deformation process (Fig. 10B–B'; cf. Phillips, 2006; Phillips et al., 2018, and references therein). Folded lower boundaries of erosional scours at the base of troughs in unit A (Fig. 3F) indicate that the erosional scours were subsequently deformed.
- (2) The presence of vertical and semi-vertical, predominantly small-scale brittle deformation (Fig. 3A) in the form of normal faults and fractures, especially in the lower unit A, may have developed post-depositionally as a result of vertical pressure from overlying sediments and their varying compaction, e.g., between two grain-size domains. Furthermore, lateral changes in compactibility could also cause structural deformation and faults formation (cf. Xu et al., 2015). The occurrence of faults and fractures also suggests that the injections (Fig. 3F) may have been forceful enough

to generate localised extension and displacement in the surrounding sediment, possibly accompanied by partial dewatering. This relationship indicates that liquefied sediments not only intruded pre-existing laminae, but also induced additional structural modifications in response to fluid escape (cf. Phillips, 2006; Phillips et al., 2018; Phillips and Evans, 2019). Furthermore, the occurrence of a set of faults and fractures in the vicinity of steeply inclined synforms and antiforms (Fig. 3A) may result from variations in sediment plasticity during folding (cf. Pisarska-Jamrozy et al., 2024). Faults occurring immediately beneath the troughs most likely developed as a result of shear stress induced by an energy of flow during the initial stage of erosional scours development. This process caused sudden and uneven compaction of the underlying sediments (Fig. 3F).

- (3) Hydrofracturing, identified in unit B (Fig. 11C), occurred when high water pressure exceeded the cohesive strength of the sediment, resulting in fracturing (cf. Ravier et al., 2014; Pisarska-Jamrozy et al., 2024; Ravier, 2024). These hydrofractures were subsequently infilled by escaping water carrying a mixture of sandy silts or silty sands, along with millimetre-sized silty clasts derived from the source layer (Fig. 11C). It is likely that the hydrofracturing was triggered in water-saturated sediments by the uneven loading of overlying deposits.
- (4) The broken-up laminae observed in the antiforms of unit B (Fig. 8A–C) result from the tearing and extension of the sediment. They developed as a consequence of sediment inhomogeneities. The broken-up laminae, visible in Fig. 9A and 11C, formed due to

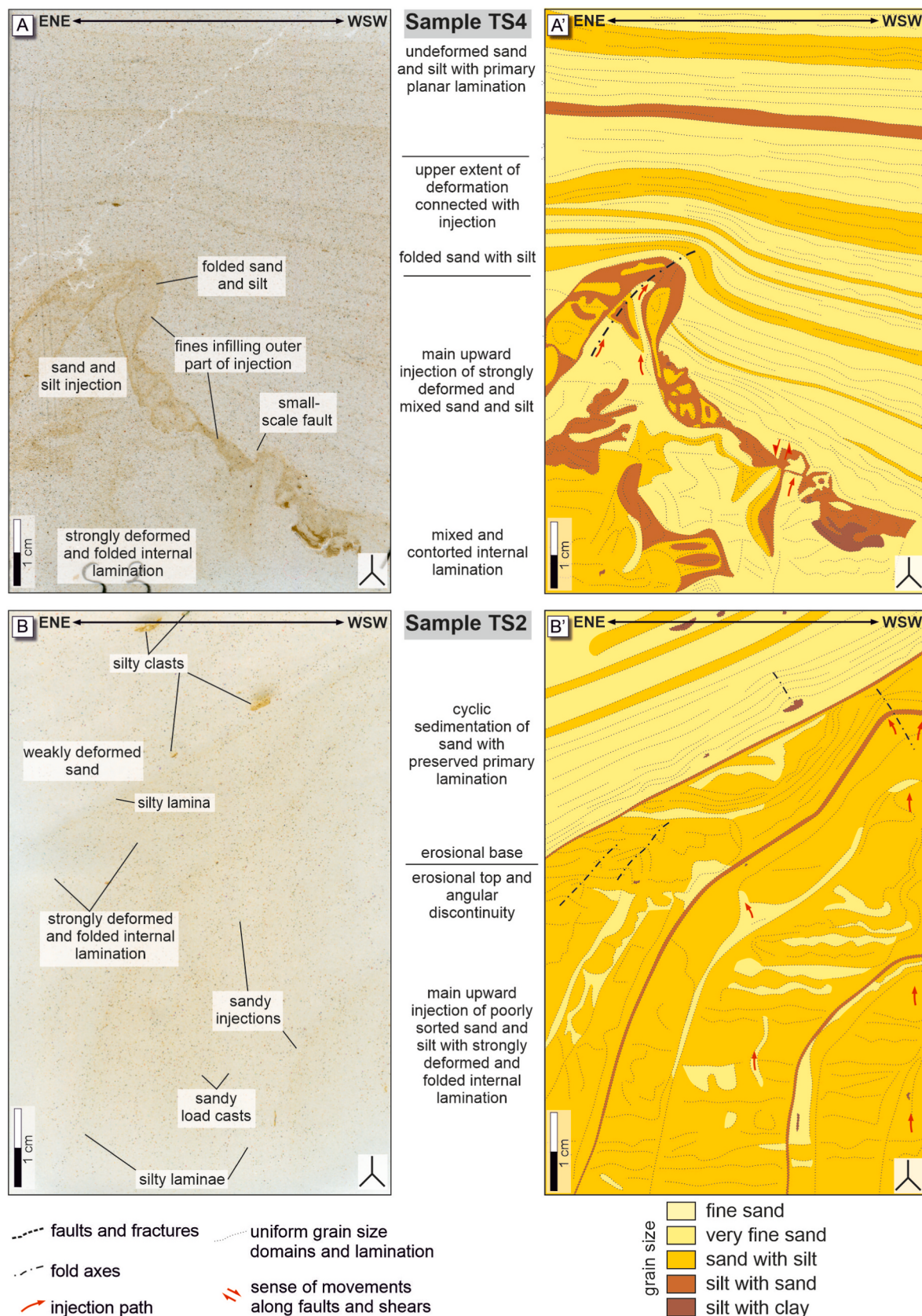


Fig. 10. High-resolution scans of the thin sections and interpretation of the microsedimentology within two samples from the Särnate study site: (A) and (A') sample TS4 that represents the contact between a mesoscale injection structure and the overlying horizontally-laminated, sand-dominated sediments of unit B; (B) and (B') sample TS2, which was collected from the erosional contact zone between the uppermost part of unit A and a trough-shaped structure with a sand-dominated infilling, located between units A and B (see Fig. 3).

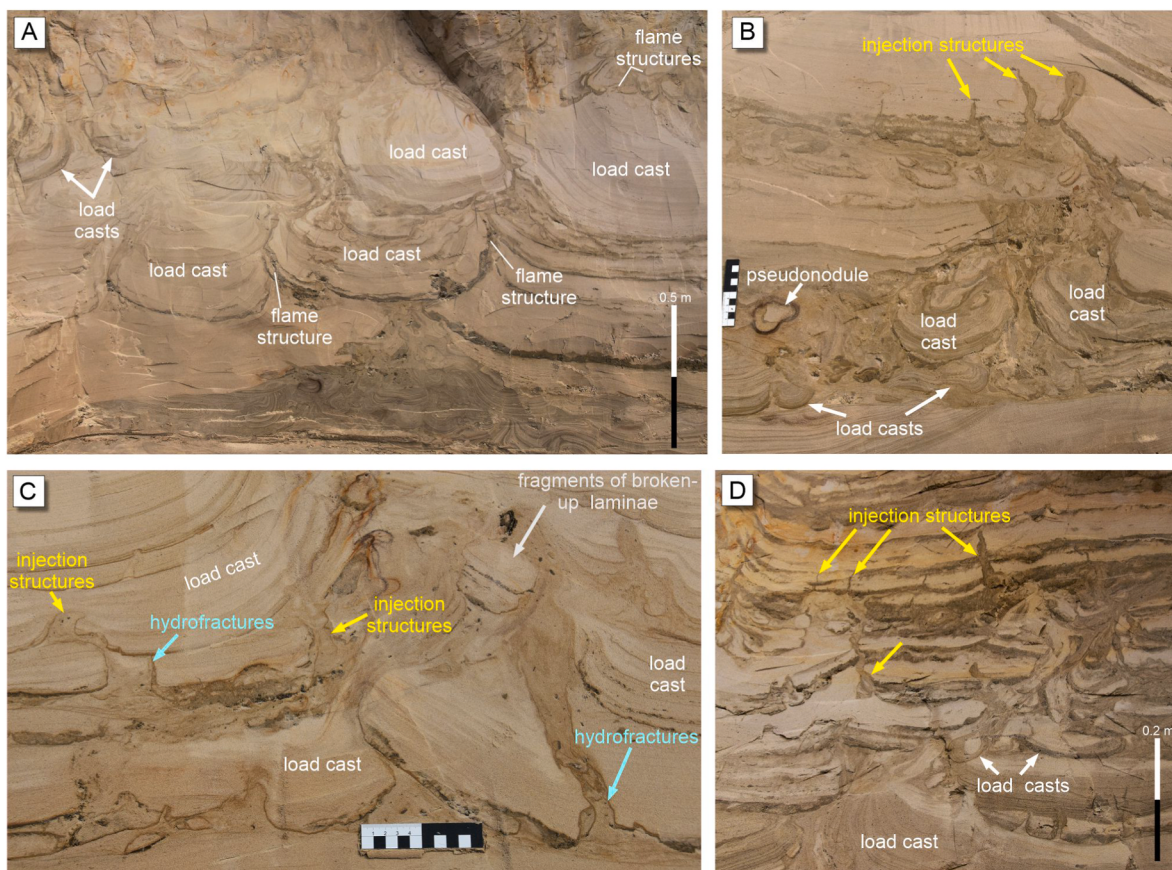


Fig. 11. Deformation structures in unit B. (A) Large-scale load casts and flame structures, suggesting multiloadings processes. (B) Load casts, pseudonodule, and injection structures in unit B. (C) Fragments of broken-up laminae, hydrofractures cutting through load casts and injection structures. (D) Injection structures and load casts with flame structures in the unit B.

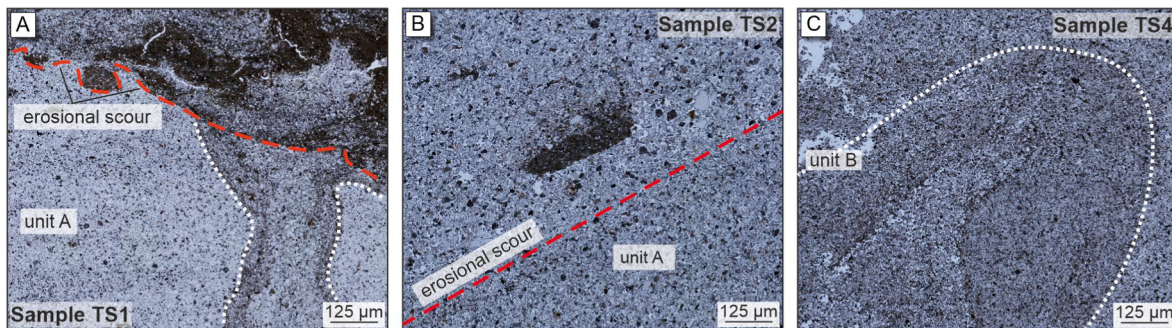


Fig. 12. Photomicrographs of selected parts of thin sections in plane-polarised light providing a detailed view of deformation structures. Red dashed lines indicate the erosional boundaries and grain-size domains within the unit A. White dotted lines indicate the outer shape of the injection structures within the unit A. For location see Figs. 6 and 10). (For interpretation of the references to colour in this figure legend, the reader is referred to the Web version of this article.)

- the injection of lower-lying liquefied sediments upwards. This process led to the cutting of the overlying laminae sets and their slight rotation.
- (5) The combined meso- and microscale observations confirm that the load casts and pseudonodules, as mature forms of load casts (Fig. 9A and 11), at the Sarnate site developed due to density contrasts and sediment liquefaction (cf. Owen and Moretti, 2008; Owen et al., 2011). These deformation processes were influenced by high pore-water pressures and sediment loading (cf. Dżułyński and Kotlarczyk, 1962; Allen, 1982; Owen, 2003; Moretti and Sabato, 2007). In the upper unit B, the complex structure of load casts may also suggest sequential formation (Fig. 3A and 11A).

This sequential development is further observed in the infilling of the injection structures, where earlier-formed load casts are present (Fig. 10B-B'). Small-scale silty load casts and pseudonodules, associated with upward-directed injections of sand, are observed in the uppermost part of thin section sample TS3 (this sample represents the deformed silty-sandy infilling of erosional scours between units A and B). These postdepositional features most likely formed due to overloading of unit B sediments (Fig. 6A-A'). Flame structures formed between load casts as upward-pressed sediments reacted to the weight of the overlying layers (Fig. 11A). Load casts and flame structures occur together

due to density equilibrium: when part of the sediment moves downward, another part is displaced upward.

(6) The injection process caused the upward bending of overlying laminae due to the passage of a water-sediment mixture induced by liquefaction (Fig. 9B–D, E and 10B–B'). The geometry of injection structures at the study sites indicates an originally upward water flow (i.e., *per ascensum*; cf. Moretti et al., 1999; Moretti, 2000). Poorer sorting of the injected sediments as well as observed finer-grained outer parts of injection structures may result from partial incorporation and mixing with surrounding sediments, requiring a relatively sudden flow, or may result from the heterogeneity of the source sediment (cf. Taylor, 1982; van der Meer et al., 2009 and cited therein; Świątek et al., 2023). Injection structures deformed adjacent sediments, bending laminae boundaries as escaping water and sediment moved through. Small-scale injections penetrated the overlying sand (lithofacies Se at Fig. 3E and F), deflecting lamination within the sand laminae. Their presence within troughs was most likely caused by shear stress exerted on the underlying sediments by a sudden and energetic flow, similar to the case of faulting and fracturing described above.

The single quartz fractures observed in thin sections may instead stem from the sediment's transport history and depositional processes rather than seismic activity (Fig. 7). Seismically induced liquefaction would typically result in more frequent and well-developed quartz fractures, as mechanical stress during seismic shaking often causes grain breakage and microcrack formation (cf. Świątek et al., 2025). Furthermore, recent studies have proposed that, under specific conditions, the presence of gold accumulations linked to earthquake-induced pressure fluctuations and fluid mobilisation can serve as a criterion for recognising seismites (Voisey et al., 2024; Świątek et al., 2025). The liquefied sediments at Särnate lack any evidence of gold particles, which weakens, though does not entirely rule out, the hypothesis that these sediments underwent earthquake-triggered liquefaction.

The timespan (Fig. 13) of the deformation processes that affected units A and B within the sedimentary succession at the Särnate site, along with their triggering mechanisms, is discussed within the broader palaeogeographical context in section 6.

5. Discussion

5.1. Liquefaction as a key driver of deformation in lagoonal sediments

The sediments of both units A and B at the Särnate site (Fig. 3A, B, 4 and 11) are highly susceptible to liquefaction, influenced by grain size distribution and the proportion of fine-grained fractions, particularly silt and sand (cf. Obermeier, 1996; Owen, 1996, 2003; Świątek et al., 2023). The sediments that undergo liquefaction, such as those filling injection structures, are poorly sorted (Fig. 8). This is consistent with the findings of Świątek et al. (2023) but contrasts with earlier results from Maltman and Bolton (2003), as well as Collinson et al. (2019). Only the sediments in loaded structures are characterised by better sorting, as also confirmed by results obtained by Świątek et al. (2023).

Liquefaction requires sediments to be water-saturated (Campbell, 2003), with a water content exceeding 90 % of liquid limit (Wang, 1979; Seed et al., 1983), which was the case for the studied depositional palaeoenvironment. The occurrence of SSDS, especially injection structures, in the subaqueous deposits at the Särnate site is strongly linked to liquefaction (cf. Nartiss et al., 2018). Liquefaction features have been documented in various coastal and lagoonal sedimentary records (Alfaro et al., 1997; Moretti and Sabato, 2007; Van Loon, 2009; Owen and Moretti, 2011; Uyanik et al., 2013; Gao et al., 2019; Üner et al., 2019; Mavroulis et al., 2021). Lagoonal environments are particularly prone to liquefaction due to their heterolithic deposits, characterised by alternating coarser (sand) and finer (silt) sediments (cf. Sims, 1975; Seed et al., 1983; Rodríguez-Pascua et al., 2000). Such depositional settings commonly experience sudden increases in interlayer pore pressure (Seed, 1979; Maltman and Bolton, 2003; Moretti and Sabato, 2007; Liang et al., 2024). In the Särnate profile, the interbedded sediments with different textures (sandy and silty layers) created ideal conditions for the development of excess pore-water pressure, promoting liquefaction and sediment deformation (Fig. 11). Water-saturated sediments, overpressure, and insufficient compaction, combined with limited permeability caused by intercalated clay and silt laminae, hindered pore-water dissipation, thereby increasing susceptibility to liquefaction (Youd, 1973; Lowe, 1976; Allen, 1982; Moretti et al., 2001; Owen, 2003; Moretti and Sabato, 2007).

5.2. Triggers of liquefaction in lagoonal sediments

Liquefaction may be triggered by various geological processes, including overloading, wave action, permafrost degradation, tsunamis, storms, meteorite impacts, or seismic shaking caused by glacial isostatic

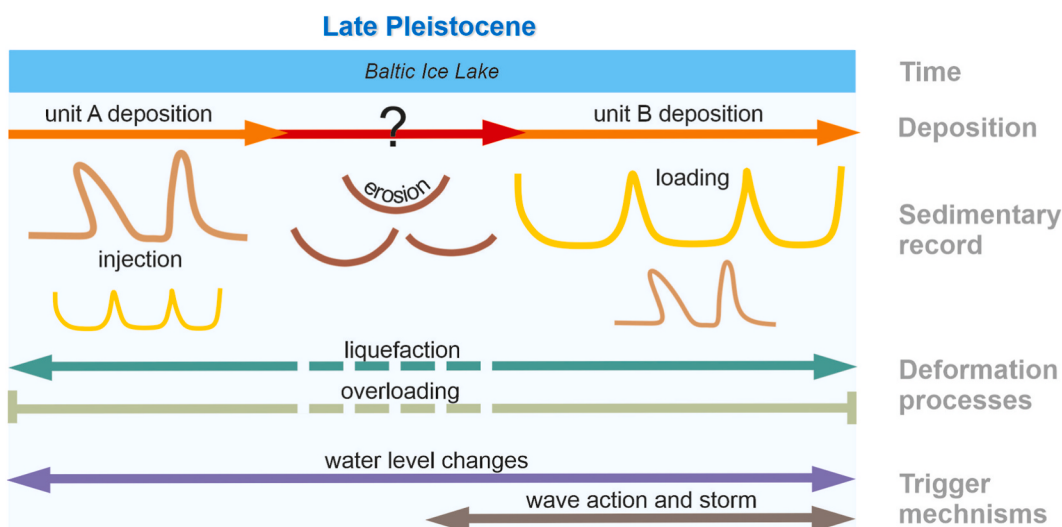


Fig. 13. Chronology of the sedimentary processes at Särnate site.

adjustments or the seismic activity of ice sheets (e.g., Allen, 1982; Obermeier, 1996; Van Loon, 2009; Owen and Moretti, 2011; Świątek and Pisarska-Jamrozy, 2025), and can contribute to the development of SSDS. Below, we discuss only those trigger mechanisms that could have occurred in the study area within the time frame corresponding to sediment deposition or the post-depositional period.

5.2.1. Fault reactivation in response to GIA

An increasing number of studies have demonstrated that earthquake-induced liquefaction plays a significant role in SSDS formation, particularly in settings with highly saturated, fine-grained sediments (cf. Hilbert-Wolf et al., 2009; Brandes et al., 2012, 2015, 2018; Moretti and Van Loon, 2014 and cited therein; Pisarska-Jamrozy et al., 2018, 2019b, 2022; Woźniak et al., 2021). One of the most commonly cited mechanisms for seismically-induced SSDS in formerly glaciated regions is the reactivation of pre-existing faults due to GIA. This process is well-documented, with evidence of Late Pleistocene and Holocene seismites (=layers with SSDS induced by seismic shaking; see Seilacher, 1969) attributed to fault reactivation, e.g., at sites across the Peribaltic region (e.g., Brandes et al., 2012, 2015, 2018; Pisarska-Jamrozy et al., 2018, 2019b, 2022, 2024; Grube, 2019a, b; Steffen et al., 2019; Belzty et al., 2021; Seidel et al., 2025).

Some diagnostic criteria for identifying seismites (cf. Hilbert-Wolf et al., 2009; Owen and Moretti, 2011; Moretti and Van Loon, 2014; Świątek et al., 2025) can be applied to the succession exposed at the Särnate site when assessing the possibility of fault reactivation as a trigger mechanism. The widespread occurrence of liquefaction structures, including injection features within susceptible sediments (Obermeier, 1996; Świątek et al., 2023; see Fig. 5) indicates rapid increases in pore-water pressure, a phenomenon commonly associated with seismically-induced liquefaction (Hilbert-Wolf et al., 2009; Owen and Moretti, 2011). Numerical modelling by Steffen et al. (2019) for the Särnate site area suggests that fault reactivation in response to ice-sheet retreat may have been possible from around 13–12 ka BP and could have continued intermittently to the present. However, despite the potential for fault reactivation as a trigger mechanism, several key criteria for recognising seismite are either not applicable or not met at the Särnate site. Unlike typical seismites, which extend over large areas in a laterally continuous manner (cf. Owen and Moretti, 2011), the deformed layers at the Särnate site often exhibit discontinuities and spatially restricted deformation zones. Secondly, the deformation structures do not display the characteristic “sandwich-like” arrangement of earthquake-related seismites (Rodríguez-Pascua et al., 2000; Owen and Moretti, 2011; Moretti and Van Loon, 2014). In many cases, deformation structures at Särnate site cut discordantly through overlying layers rather than being confined within a single layer bounded by undisturbed layers above and below. This feature may result from the fact that all sediments with SSDS at Särnate site were highly susceptible to liquefaction during deposition. Moreover, no specific cracks, fractured quartz grains (Fig. 7) were observed, as had been suggested in seismically affected sediments by Świątek et al. (2025). This pattern of deformation suggests that processes other than seismic shaking may be responsible for the formation of the observed structures. Furthermore, no direct evidence of fault displacement in the area within the relevant time frame has been documented. Without structural mapping or geophysical confirmation of neotectonic faulting, attributing the observed deformations solely to seismic activity remains highly speculative and cannot be substantiated with the currently available data.

5.2.2. Icequakes

Icequakes, seismic events generated by glacial dynamics, are increasingly recognised as a potential trigger for liquefaction and SSDS in proglacial environments (e.g., Ekström et al., 2003; Nettles and Ekström, 2010; Phillips et al., 2018; Hart et al., 2019). Recent studies have shown that icequakes can result from various mechanisms, including rapid basal slip, ice front fluctuations, hydraulic forcing, and

stick-slip behaviour at the glacier bed (Podolskiy and Walter, 2016; Lipovsky and Dunham, 2016). These processes can generate seismic shaking strong enough to induce liquefaction in water-saturated near-surface sediments, particularly in areas directly influenced by an active ice sheet margin (Ekström et al., 2006; Tsai et al., 2008; Walter et al., 2013). Modern examples from Greenland and Antarctica show that significant seismic energy can be transmitted through glacially influenced sediments for hundreds of kilometres from an ice front (Nettles and Ekström, 2010; Walter et al., 2013). However, no studies have yet reported the maximum distance from an epicentre at which liquefaction can occur in sediments.

At the Särnate site, certain SSDS resemble those observed in icequake-related seismites described in Pleistocene proglacial settings (cf. Woźniak et al., 2021 and cited therein). Although seismically induced SSDS caused by icequakes were identified at the Baltmuiža site, located approximately 25 km southwest of the Särnate site (Fig. 1B; Woźniak et al., 2021), the deformed sediments at Baltmuiža are older, dated by OSL between 30.5 ± 1.8 ka and 26.3 ± 1.5 ka, than those at Särnate. Therefore, the deformation structures at the two sites should not be correlated. Based on reconstructions of the FIS extent, OSL dating, and the stratigraphic context, the ice sheet around 13.8 ± 1.0 and 12.8 ± 1.0 ka BP was most likely too distant (70–80 km; Fig. 1A) to have triggered liquefaction and the development of SSDS at the Särnate site.

5.2.3. Storm and wave action

The nearshore depositional conditions prevailing during the deposition of unit B at the Särnate site provided a favourable environment for sediment liquefaction induced by storms or wave action. High-energy hydrodynamic processes, such as storm surges, have been documented as potential triggers of liquefaction and SSDS formation in coastal and nearshore settings (Dott and Bourgeois, 1982; Zen and Yamazaki, 1990; Molina et al., 1998; Sumer et al., 2006). These processes can rapidly increase pore pressure in water-saturated sediments, leading to liquefaction.

However, it is important to note that the Särnate succession lacks hummocky cross-stratification (HCS, i.e., tempestites; Dott and Bourgeois, 1982), bioturbations and bi-directional flow indicators, features that are typically characteristic of storm deposits. This absence may be explained by the sediments at the Särnate site being too fine (fine-grained sands and silts) to preserve HCS, which more commonly forms in coarser sands (Walker and Plint, 1992; Collinson et al., 2019). It is also possible that any sedimentary indicators of direct storm activity that may have originally developed were later removed by erosional processes associated with lake-level fluctuations or wave- and storm-driven scouring. The presence of rip-up clasts within the infilling of troughs suggests current erosion of the lower unit A (Fig. 3), likely intensified by storm and wave action in the area. Furthermore, water-level drawdown may have been responsible for destabilising the delicate equilibrium of sandy-silt-clay laminated sediments, leading to the development of liquefaction features, density loading, and SSDS formation at the Särnate site. Potter and Pettijohn (1977) observed that even high-porosity sands, when deposited onto less porous, plastic clayey silt layers, can contribute to sediment destabilisation and the development of SSDS. Poor sorting and sediment mixing, observed both at the mesoscale and in thin section analysis, may be linked to these water level changes.

Considering the above evidence, water drainage, along with storm and wave action, should be considered as possible triggers of liquefaction and SSDS development at the Särnate site.

5.2.4. Sediment overloading

Sediment overloading during the uneven deposition of sediments is one of the major processes responsible for SSDS formation (Dżułyński and Kotlarczyk, 1962; Allen, 1982; Van Loon, 2009). This mechanism is known to induce liquefaction even in the absence of seismic shocks (Moretti and Sabato, 2007). This phenomenon is common across various

depositional settings, including fluvial, lacustrine, deltaic, and marine environments (Beck et al., 1996; Alfaro et al., 1997; Gao et al., 2019; Üner et al., 2019). Environmental conditions typical of lagoonal and possibly adjacent lacustrine or floodplain settings are particularly conducive to rapid sedimentation events (e.g., Allen, 1982; Seed et al., 1983). These environments often experience fluctuating sedimentation

rates, leading to periodic overloading and instability (cf. Sims, 1975; Oliveira et al., 2011; Stárková et al., 2015).

The diverse SSDS observed at the Särnate site strongly supports sediment overloading as the primary triggering mechanism responsible for their development (cf. Moretti et al., 1999). The irregular distribution of SSDS within the sedimentary succession, where load features are

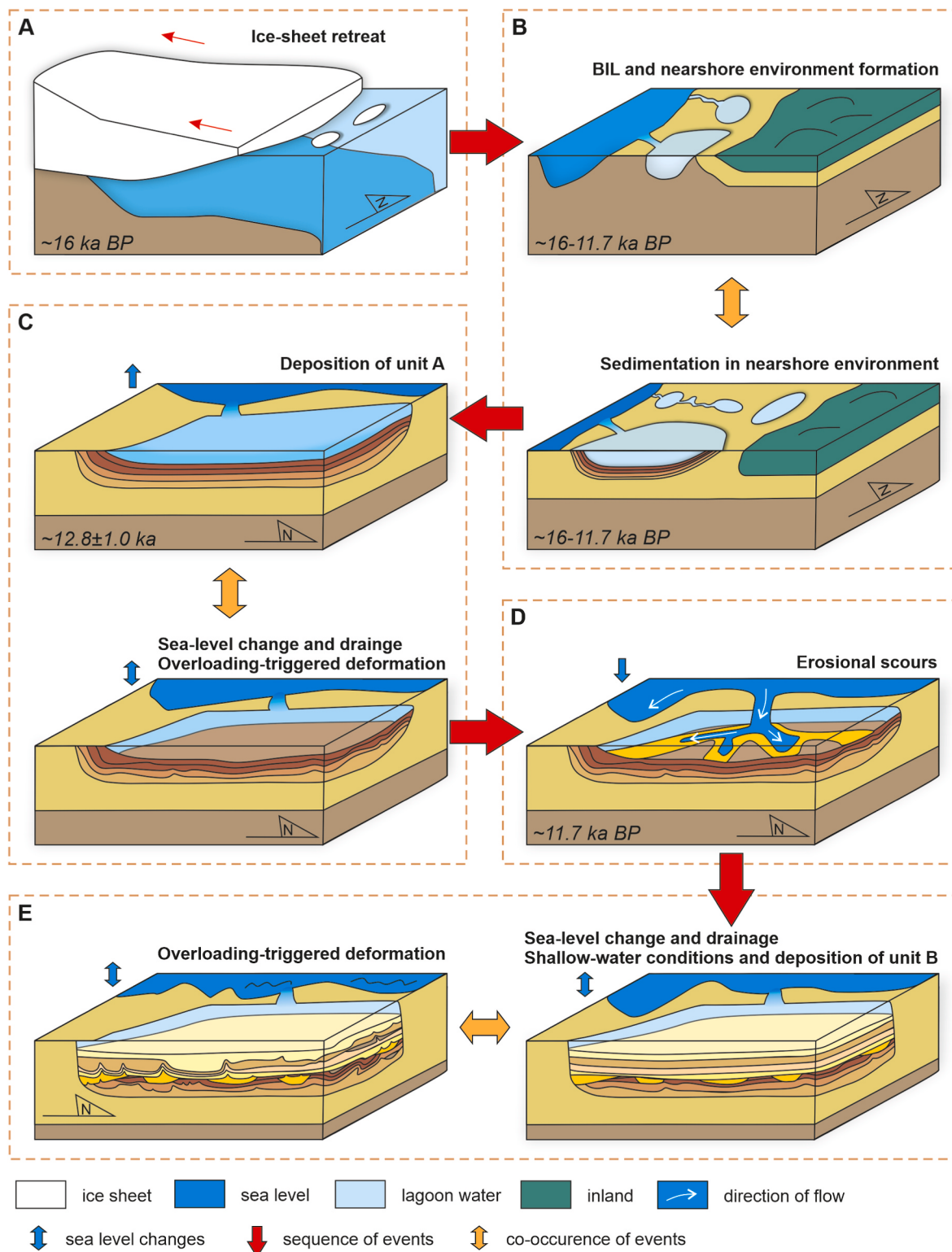


Fig. 14. Schematic palaeogeographic model illustrating the evolution of the Särnate site sedimentary succession through key depositional and erosional processes (not to scale).

concentrated in some areas while injection structures dominate elsewhere, suggests uneven overloading, which facilitates the rise in pore-water pressure within sediment layers (cf. Allen, 1982) and leads to variable sedimentary responses (see Fig. 3).

The larger and more pronounced SSDS observed in the upper unit B, compared to the less-developed structures in the lower unit A (Fig. 3), suggests that the lower unit A gradually adjusted to the deformation caused by the overlying unit B (Fig. 11). The inconsistency in liquefied sediment layer thickness and deformation intensity further reflects highly variable depositional rates (cf. Gao et al., 2019).

Sediment overloading may have played a significant role in triggering liquefaction and SSDS formation at the Sārnate site, particularly when combined with other triggers.

6. Palaeogeographic evolution of the nearshore succession at the Sārnate site

The retreat of the FIS from the study area during the Late Pleistocene, which began approximately 16 ka BP (cf. Houmark-Nielsen and Kjær, 2003; Stroeven et al., 2016), triggered significant environmental changes, including the formation of the BIL between 16 and 11.7 ka BP (Andrén et al., 2011). OSL dating indicates that sediments from unit A were deposited around 13.8 ± 1.0 ka and 12.8 ± 1.0 ka (Fig. 4). Palaeogeographic reconstructions suggest that around 13.3 cal ka BP the FIS margin was located near the Palivere position, approximately 70–80 km north of Sārnate (Fig. 1A). According to palaeogeographic models (Rosentau et al., 2009; Vassiljev and Saarse, 2013), the deep water conditions existed in the Sārnate area around c. 13.3 cal ka BP with the relative shore level (RSL) of the BIL approximately 35 m a.s.l.

As the FIS retreated northwards, the first drainage event of the BIL (cf. Björck, 1995) occurred at 12.87 cal ka BP (Muschiello et al., 2016) resulting in a water level drop of c. 20 m as recorded from the Arkona Basin (Bennike and Jensen, 2013) or c. 10–15 m as recorded from the Blekinge area (Björck, 1995). The rhythmically deposited silty sand, sandy silt, and silt of unit A (lithofacies FSh, SFh, Fh; Figs. 3 and 14) were likely deposited during or shortly after the drainage event, when increased erosion of exposed glacial landforms in the east supplied significant quantities of sandy and silty sediments, later deposited in the nearshore environment. The water level in the Sārnate area following the initial drainage event remains poorly understood. RSL reconstructions suggest that BIL water levels at the Sārnate area were around 35 m a.s.l. at 13.3 cal ka BP and around 30 m a.s.l. at 11.7 cal ka BP, prior to the first and final drainage events, respectively (Rosentau et al., 2009; Vassiljev and Saarse, 2013). Considering the 20–10 m water level drop and some contribution from isostatic uplift since 13.3 cal ka BP, the RSL in Sārnate was likely in the range of 25 and 10 m a.s.l. Consequently, nearshore conditions with increased sediment input were established in the study area for the first time during the development of the BIL.

Isolated deformation structures, such as injection features and load casts, identified within unit A may have formed under conditions favourable to liquefaction in water-saturated sediments, as well as due to overloading associated with the progressive accumulation of fine-grained sediments. The sediments of the unit A partly eroded probably during the second and final (25 m) drainage event of the BIL at 11.7 cal ka BP (Björck, 1995; Andrén et al., 2011), as evidenced by erosional scours at the base of troughs, where rip-up clasts have been identified (Fig. 3). During the final drainage the water level was lowered from 30 to 5 m a.s.l. leading to the establishment of shallow-water conditions in the Sārnate area.

The drainage, which caused the development of erosional scours, affected the underlying sediments through shear stress generated by flow currents at the base of the troughs. This process likely led to the formation of injection structures within the trough infill, as well as the development of faults and fractures in the underlying layers. During or just following the drainage event, the horizontally-laminated sands, silty

sands, and silts (lithofacies association Sh, SFh, Fh) of unit B were deposited in a shallow nearshore environment.

The sediments of the upper unit B, being coarser than those in unit A, were deposited under shallower nearshore conditions following the drainage of the BIL, suggesting that storm and wave action may have influenced the sedimentary succession. The presence of coarser sediments and an increased sedimentation rate led to overloading, which played a role in the development of deformation in both units A and B. This overloading resulted in uneven pressure on the underlying sediments, causing them to undulate and leading to the formation of synforms and antiforms, as well as brittle deformation such as faults and fractures. The sediments in unit B were prone to liquefaction; therefore, storm and wave action may have contributed to the development of liquefaction conditions, resulting in the formation of injection structures and load casts.

The absence of sediments younger than those deposited during the BIL stage, may suggest subsequent coastal or fluvial erosion processes that removed later Holocene-age deposits.

7. Conclusions

The following conclusions can be drawn.

1. The Sārnate site in western Latvia contains well-developed soft-sediment deformation structures (SSDS) within Late Pleistocene nearshore deposits, providing evidence of past liquefaction linked to Baltic Ice Lake (BIL) drainage event.
2. The drainage event contributed to conditions favourable for liquefaction and fluidisation in water-saturated silty sands and sandy silts, leading to sediment destabilisation and the formation of SSDS, like injection structures, load structures (load casts, pseudonodules) and flame structures.
3. Overloading, which exerted vertical pressure on the underlying sediments, was responsible for the uneven compaction of the water-saturated layers beneath, leading to the development of synforms and antiforms, as well as fragments of broken-up laminae in sediments characterised by lower plasticity. The downward force of the overlying sediments may also have contributed to the formation of isolated injection structures and hydrofractures.
4. High pore-water pressure within the sedimentary succession at the Sārnate site can be reconstructed on the base of generally abruptly-developed hydrofractures. Erosional scours and sedimentary features at the site further indicate episodes of hydrodynamic reworking related to water level changes and barrier breaching, contributing to the sedimentary complexity and potential remobilisation of previously deposited and deformed sediments.
5. The distribution and morphology of SSDS, such as folds, load casts, pseudonodules, disrupted laminae, hydrofractures, and injection structures, indicate deformation caused by water-level fluctuations in the BIL. These fluctuations likely caused water drainage events and changes in pore-water pressure, resulting in liquefaction, with wave activity and overloading acting as additional contributing factors. The most probable trigger mechanism for the observed palaeoliquefaction features was overloading caused by the uneven deposition of sediments, leading to density instability and insufficient gravitational equilibrium within the stratified layers.
6. The spatial complexity of SSDS at the Sārnate site suggests that local sedimentary conditions, recorded as the grain size contrasts, permeability variations, and the presence of confining layers, played a crucial role in controlling deformation processes. These findings emphasize the significance of site-specific sedimentological characteristics in determining liquefaction susceptibility and deformation styles.
7. Our results contribute to the broader understanding of palaeoliquefaction in nearshore settings, emphasizing the need for multi-proxy approaches (sedimentological, microstructural,

- geochronological) to distinguish between seismic and non-seismic triggers of deformation.
8. To refine the interpretation of liquefaction triggers, further investigations should include geotechnical analyses of sediment strength properties, high-resolution chronological control, and comparisons with other deformation sites across the Baltic Sea region.

Author contributions

Małgorzata Pisarska-Jamrozy: Conceptualization, Methodology, Validation, Resources, Data curation, Writing – original draft, Writing – review & editing, Visualization, Supervision, Project administration, Funding acquisition. Szymon Belzyt: Investigation, Conceptualization, Methodology, Validation, Resources, Data curation, Writing – review & editing, Visualization. Māris Nartišs: Investigation, Writing – review & editing. Albertas Bitinas: Investigation, Writing – review & editing. Barbara Woronko: Investigation, Writing – review & editing. Alar Rosentau: Writing – review & editing. Szymon Świątek: Investigation, Conceptualization, Methodology, Validation, Resources, Data curation, Writing – review & editing, Visualization.

Declaration of competing interest

The authors declare that they have no known competing financial interests or personal relationships that could have appeared to influence the work reported in this paper.

Acknowledgments

The study has been financially supported by grants No. 2015/19/B/ST10/00661 (GREBAL project), 2019/35/N/ST10/03401 and 2023/49/N/ST10/00282 from the National Science Centre, Poland. The work of Māris Nartišs has been partially supported from the performance-based funding of the University of Latvia. The authors thank the reviewer and the editor for their constructive comments which significantly contributed to improving the manuscript.

Appendix A. Supplementary data

Supplementary data to this article can be found online at <https://doi.org/10.1016/j.quascirev.2025.109622>.

Data availability

All data and/or code is contained within the submission.

References

- Alfaro, P., Moretti, M., Soria, J.M., 1997. Soft-sediment deformation structures induced by earthquakes (seismites) in Pliocene lacustrine deposits (Guadix-Baza Basin. Central Betic Cordillera). *Eclogae Geol. Helv.* 90, 531–540.
- Allen, J.R.L., 1982. *Sedimentary Structures: Their Character and Physical Basis*. Elsevier, pp. 1–593.
- Allen, J.R.L., 1987. Reworking of muddy intertidal sediments in the severn estuary, Southwestern U.K. A preliminary survey. *Sed. Geol.* 50, 1–23. [https://doi.org/10.1016/0037-0738\(87\)90026-1](https://doi.org/10.1016/0037-0738(87)90026-1).
- Alsop, G.I., Marco, S., 2011. Soft-sediment deformation within seismogenic slumps of the Dead Sea Basin. *J. Struct. Geol.* 33, 433–457. <https://doi.org/10.1016/j.jsg.2011.02.003>.
- Andrén, T., Björck, S., Andrén, E., Conley, D., Zillén, L., Anjar, J., 2011. The development of the Baltic Sea basin during the last 130 ka. In: Harff, J., Björck, S., Hoth, P. (Eds.), *The Baltic Sea Basin*. Springer, Heidelberg, pp. 75–98. https://doi.org/10.1007/978-3-642-17220-5_4.
- Ashley, G.M., 1975. Rhythmic sedimentation in glacial Lake Hitchcock, Massachusetts-Connecticut. In: Jopling, A.V., McDonald, B.V. (Eds.), *Glaciolacustrine Sedimentation*, vol. 23. Society of Economic Paleontologists and Mineralogists Special Paper, pp. 304–320. <https://doi.org/10.2110/pec.75.23.0304>.
- Bádenas, B., Aurell, M., Gasca, J.M., 2018. Facies model of a mixed clastic-carbonate, wave-dominated open-coast tidal flat (Tithonian–Berriasiian, north-east Spain). *Sedimentology* 65, 1631–1666. <https://doi.org/10.1111/sed.12441>.
- Beck, C., Manalt, F., Chapron, E., Van Rensbergen, P., De Batist, M., 1996. Enhanced seismicity in the early post-glacial period: Evidence from the post-Würm sediments of Lake Annecy, northwestern Alps. *J. Geodyn.* 22 (1–2), 155–171. [https://doi.org/10.1016/0264-3707\(96\)00013-6](https://doi.org/10.1016/0264-3707(96)00013-6).
- Belzyt, S., Pisarska-Jamrozy, M., Bitinas, A., Woronko, B., Phillips, E.R., Piotrowski, J.A., Jusienė, A., 2021. Repetitive Late Pleistocene soft-sediment deformation by seismicity-induced liquefaction in north-western Lithuania. *Sedimentology* 68, 3033–3056. <https://doi.org/10.1111/sed.12441>.
- Bennike, O., Jensen, J.B., 2013. A Baltic Ice Lake lowstand of latest Allerød age in the Arkona Basin, southern Baltic Sea. *GEUS Bull* 28, 17–20. <https://doi.org/10.34194/geusb.v28.4710>.
- Best, J.L., Kostaschuk, R.A., Peakall, J., Villard, P.V., Franklin, M., 2005. Whole flow field dynamics and velocity pulsing within natural sediment-laden underflows. *Geology* 33, 765–768. <https://doi.org/10.1130/G21516.1>.
- Björck, S., 1995. A review of the history of the Baltic Sea, 13.0–8.0 ka BP. *Quat. Int.* 27, 19–40. [https://doi.org/10.1016/1040-6182\(94\)00057-C](https://doi.org/10.1016/1040-6182(94)00057-C).
- Brandes, C., Winsemann, J., Roskosch, J., Meinen, J., Tanner, D.C., Frechen, M., Steffen, H., Wu, P., 2012. Activity along the Osning Thrust in Central Europe during the Lateglacial: ice-sheet and lithosphere interactions. *Quat. Sci. Rev.* 38, 49–62. <https://doi.org/10.1016/j.quascirev.2012.01.021>.
- Brandes, C., Steffen, H., Steffen, R., Wu, P., 2015. Intratice seismicity in northern Central Europe is induced by the last glaciation. *Geology* 43, 611–614. <https://doi.org/10.1130/G36710.1>.
- Brandes, C., Steffen, H., Sandersen, P.B.E., Wu, P., Winsemann, J., 2018. Glacially induced faulting along the NW segment of the Sorgenfrei-Tornquist Zone, northern Denmark: implications for neotectonics and Lateglacial fault-bound basin formation. *Quat. Sci. Rev.* 189, 149–168. <https://doi.org/10.1016/j.quascirev.2018.03.036>.
- Brandes, C., Polom, U., Winsemann, J., Sandersen, P.B., 2022. The near-surface structure in the area of the Borgum fault, Sorgenfrei-Tornquist Zone, northern Denmark: implications for fault kinematics, timing of fault activity and fault control on tunnel valley formation. *Quat. Sci. Rev.* 289, 107619. <https://doi.org/10.1016/j.quascirev.2022.107619>.
- Brangulis, A., Kanev, S., 2002. *Latvijas Tektonika [Tectonics of Latvia]*. Valsts Geoloģijas Dienests, Riga, p. 50 (in Latvian, with English summary).
- Breijers, E., Kalińska, E., Krievāns, M., 2023. Detecting the displacement of the Baltic basin's ancient shorelines by clustering of terrain and distance data along the glacioisostatic uplift axis. *Séances Soc. Préhist. Fr* 19, 159–172.
- Brodzikowski, K., Van Loon, A.J., 1991. Glacigenic sediments. *Dev. Sedimentol.* 19, 674. Elsevier, Amsterdam.
- Bronikowska, M., Pisarska-Jamrozy, M., Van Loon, A.J., 2021. First attempt to model numerically seismically-induced soft-sediment deformation structures – a comparison with field examples. *Geol. Q.* 65, 60. <https://doi.org/10.7306/gq.1629>.
- Campbell, C.S., 2003. Rapid granular flows. *Annu. Rev. Fluid Mech.* 22, 57–90. <https://doi.org/10.1146/annurev.fl.22.010190.000421>.
- Casagrande, A., 1976. Liquefaction and cyclic deformation of sands: a critical review. *Harvard Soil Mech. Ser.* 88, 1–26.
- Collinson, J.D., Mountney, N., Thompson, D.B., 2019. *Sedimentary Structures*, fourth ed. Dunedin Academic Press, p. 352.
- Davies, N., Turner, P., Sansom, I.J., 2004. Soft-sediment deformation structures in the Late Silurian Stubdal Formation: the result of seismic triggering. *Nor. J. Geol.* 85, 233–243.
- Dott, R.H., Bourgeois, J., 1982. Hummocky stratification: significance of its variable sequences. *Geol. Soc. Am. Bull.* 93, 663–680.
- Dreimanis, A., Kärklin, O.L., 1997. Latvia. In: Encyclopedia of European and Asian Regional Geology. Encyclopedia of Earth Science. Springer, Dordrecht. https://doi.org/10.1007/1-4402-4495-X_59.
- Džułyński, S., 1965. New data on experimental production of sedimentary structures. *J. Sediment. Petrol.* 35, 196–212. <https://doi.org/10.1306/74D7121C-2B21-11D7-8648000102C1865D>.
- Džułyński, S., Kotlarczyk, J., 1962. O pogrzęniętych pregach falistych (ripplemarkach) [On load-casted ripples]. *Ann. Soc. Geol. Pol.* 32, 147–160.
- Ekström, G., Nettles, M., Tsai, V.C., 2006. Seasonality and increasing frequency of Greenland glacial earthquakes. *Science* 311, 1756–1758. <https://doi.org/10.1126/science.1122112>.
- Ekström, G., Nettles, M., Abers, G.A., 2003. Glacial earthquakes. *Science* 302, 622–624. <https://doi.org/10.1126/science.1088057>.
- Folk, R.L., 1954. The distinction between grain size and mineral composition in sedimentary rock nomenclature. *J. Geol.* 62, 344–359. <https://doi.org/10.1086/626171>.
- Folk, R.L., Ward, W., 1957. Brazos River bar: a study and mineral composition in sedimentary rock nomenclature. *J. Sediment. Petrol.* 27, 3–26. <https://doi.org/10.1306/74D70646-2B21-11D7-8648000102C1865D>.
- Friedman, G., Sanders, J., 1978. *Principles of Sedimentology*. Wiley, New York, p. 808.
- Gao, Y., Jiang, Z., Best, J.L., Liu, S., Zhang, J., 2019. Small- and large-scale soft-sediment deformations in a Triassic lacustrine delta caused by overloading and seismicity in the Ordos Basin, Central China. *Mar. Petrol. Geol.* 103, 126–149. <https://doi.org/10.1016/j.marpgeo.2019.02.009>.
- Gilbert, R., Crookshanks, S., Hodder, K.R., Spagnol, J., Stull, R.B., 2006. The record of an extreme flood in the sediments of montane Lillooet Lake, British Columbia: implications for paleoenvironmental assessment. *J. Paleolimnol.* 35, 737–745. <https://doi.org/10.1007/s10933-005-5152-8>.
- Gibert, L., Alfaro, P., García-Tortosa, F.J., Scott, G., 2011. Superposed deformed beds produced by single earthquakes (Tecopa Basin, California): insights into paleoseismology. *Sediment. Geol.* 235, 148–159. <https://doi.org/10.1016/j.sedgeo.2010.08.003>.

- Grinbergs, E., 1957. The late glacial and postglacial history of the coast of the Latvian SSR. *Publ. House Acad. Sci. Latv. SSR* 122. Riga.
- Grollimund, B., Zoback, M., 2000. Post glacial lithospheric flexure and induced stresses and pore pressure changes in the northern North Sea. *Tectonophysics* 327, 61–81. [https://doi.org/10.1016/S0040-1951\(00\)00162-1](https://doi.org/10.1016/S0040-1951(00)00162-1).
- Grube, A., 2019a. Palaeoseismic structures in Quaternary sediments of Hamburg (NW Germany), earthquake evidence during the younger Weichselian and Holocene. *Int. J. Earth Sci.* 108, 845–861. <https://doi.org/10.1007/s00531-019-01681-2>.
- Grube, A., 2019b. Palaeoseismic structures in Quaternary sediments, related to an assumed fault zone north of the Permian Peissen-Gnutz salt structure (NW Germany) – neotectonic activity and earthquakes from the Saalian to the Holocene. *Geomorphology* 328, 15–27. <https://doi.org/10.1016/j.geomorph.2018.12.004>.
- Hart, J.K., Martinez, K., Basford, P.J., Clayton, A.I., Robson, B.A., Young, D.S., 2019. Surface melt driven summer diurnal and winter multi-day stick-slip motion and till sedimentology. *Nat. Commun.* 10, 1599. <https://doi.org/10.1038/s41467-019-10947-6>.
- Hilbert-Wolf, H.L., Simpson, E.L., Simpson, W.S., Tindall, S.E., Wizevich, M.C., 2009. Insights into syndepositional fault movement in a foreland basin; trends in seismites of Upper Cretaceous Wahweap Formation, Kaiparowits Basin, Utah, USA. *Basin Res.* 21, 856–871. <https://doi.org/10.1111/j.1365-2117.2009.00398.x>.
- Hoffmann, G., Reicherter, K., 2011. Soft-sediment deformation of Late Pleistocene sediments along the southwestern coast of the Baltic Sea (NE Germany). *Int. J. Earth Sci.* 101, 351–363. <https://doi.org/10.1007/s00531-010-0633-z>.
- Horváth, Z., Michéli, E., Mindszenty, A., Berényi-Üveges, J., 2005. Soft-sediment deformation structures in Late Miocene–Pleistocene sediments on the pediment of the Mátra Hills (Visonta, Atkár, Verseg): cryoturbation, load structures or seismites? *Tectonophysics* 410, 81–95. <https://doi.org/10.1016/j.tecto.2005.08.012>.
- Houmark-Nielsen, M., Kjær, H.K., 2003. Southwest Scandinavia, 40–15 kyr BP: palaeogeography and environmental change. *J. Quat. Sci.* 18, 769–786. <https://doi.org/10.1002/jqs.802>.
- Huang, Y., Yu, M., 2013. Review of soil liquefaction characteristics during major earthquakes of the twenty-first century. *Nat. Hazards* 65, 2375–2384. <https://doi.org/10.1007/s11069-012-0433-9>.
- Johnston, A.C., 1987. Suppression of earthquakes by large continental ice sheets. *Nature* 330, 467–469. <https://doi.org/10.1038/330467a0>.
- Jones, A.P., Omoto, K., 2000. Towards establishing criteria for identifying trigger mechanisms for soft-sediment deformation: a case study of Late Pleistocene lacustrine sands and clays, Onikobe and Nakayamadaira Basins, northeastern Japan. *Sedimentology* 47, 1211–1226. <https://doi.org/10.1046/j.1365-3091.2000.00355.x>.
- Kalnīņa, L., Čerīņa, A., Bērziņš, V., 2019. Palaeo-geographic changes in the Sārnate former lagoon area. *Ģeogr. Raksti Folia Geogr.* 17, 7–13. <https://doi.org/10.22364/fg.17.1>.
- Kongsen, S., Phantuwongraj, S., Choowong, M., 2021. Distinguishing late Holocene storm deposit from shore-normal beach sediments from the Gulf of Thailand. *Front. Earth Sci.* 9, 625926. <https://doi.org/10.3389/feart.2021.625926>.
- Leckie, D., 1988. Wave-formed, coarse-grained ripples and their relationship to hummocky cross-stratification. *J. Sediment. Res.* 58, 607–622. <https://doi.org/10.1306/212F8E04-2B24-11D7-8648000102C1865D>.
- Liang, L., Lu, Z., Zhang, Q., Tian, H., Dai, F., Jiang, H., 2024. Shaking table simulation of soft sediment deformation structures in lacustrine sediments. *Sediment. Geol.* 472, 106756. <https://doi.org/10.1016/j.sedgeo.2024.106756>.
- Lipovsky, B.P., Dunham, E.M., 2016. Tremor during ice-stream stick slip. *Cryosphere* 10, 385–399. <https://doi.org/10.5194/tc-10-385-2016>.
- Lowe, D.R., 1976. Subaqueous liquefied and fluidized sediment flows and their deposits. *Sedimentology* 23, 285–308. <https://doi.org/10.1111/j.1365-3091.1976.tb0051.x>.
- Maltman, A.J., Bolton, A., 2003. How sediments become mobilized. In: Van Rensbergen, R., Hillis, R.R., Maltman, A.J., Morley, C.K. (Eds.), *Subsurface Sediment Mobilization*, vol 216, pp. 9–20. Geol. Soc. Lond. Spec. Publ.
- Mavroulis, S., Lekkas, E., Carydis, P., 2021. Liquefaction phenomena induced by the 26 November 2019, Mw = 6.4 Durrës (Albania) earthquake and liquefaction susceptibility assessment in the affected area. *Geosciences* 11, 1–30. <https://doi.org/10.3390/geosciences11050215>.
- McCalpin, J., Ferrario, F., Figueiredo, P., Livio, F., Grützner, Ch., Pisarska-Jamrozy, M., Quigley, M., Reicherter, K., Rockwell, T., Štěpančíková, P., Táborík, P., 2023. New developments in onshore paleoseismic methods, and their impact on Quaternary tectonic studies. *Quat. Int.* 664, 59–76. <https://doi.org/10.1016/j.quaint.2023.03.008>.
- Menzies, J., van der Meer, J.J.M., 2018. Micromorphology and microsedimentology of glacial sediments. In: Menzies, J., van der Meer, J.J.M. (Eds.), *Past Glacial Environments*, second ed. Elsevier, Amsterdam, pp. 753–806. <https://doi.org/10.1016/B978-0-08-100524-8.00036-1>.
- Miall, A.D., 1977. A review of braided river depositional environment. *Earth Sci. Rev.* 13, 1–62. [https://doi.org/10.1016/0012-8252\(77\)90055-1](https://doi.org/10.1016/0012-8252(77)90055-1).
- Miall, A.D., 1985. Architectural-element analysis: a new method of facies analysis applied to fluvial deposits. *Earth Sci. Rev.* 22, 261–308. [https://doi.org/10.1016/0012-8252\(85\)90001-7](https://doi.org/10.1016/0012-8252(85)90001-7).
- Misans, J.P., Brangulis, A.P., 1979. *Geologicheskoe Stroenie i Poleznye Iskopaemye Latvii [Geology and Mineral Resources of Latvia]*. Zinatne, Riga, p. 538 (in Russian).
- Modliński, Z., Jacyna, J., Kaney, S., Khubaldikov, A., Laskova, L., Laskovas, J., Lendzion, K., Mikazane, I., Pomeranceva, R., 1999. Palaeotectonic evolution of the Baltic Synclise during the early Palaeozoic as documented by palaeothickness maps. *Geol. Q.* 43, 285–296.
- Molina, J.M., Alfaro, P., Moretti, M., Soria, J.M., 1998. Soft-sediment deformation structures induced by cyclic stress of storm waves in tempestites (Miocene, Guadalquivir Basin, Spain). *Terra Nova* 10, 145–150. <https://doi.org/10.1046/j.1365-3121.1998.00183.x>.
- Moretti, M., 2000. Soft-sediment deformation structures interpreted as seismites in middle-late Pleistocene aeolian deposits (Apulian foreland, southern Italy). *Sediment. Geol.* 135, 167–179. [https://doi.org/10.1016/S0037-0738\(00\)00070-1](https://doi.org/10.1016/S0037-0738(00)00070-1).
- Moretti, M., Alfaro, P., Caselles, O., Canas, J.A., 1999. Modelling seismites with a digital shaking table. *Tectonophysics* 304, 369–383. [https://doi.org/10.1016/S0040-1951\(98\)00289-3](https://doi.org/10.1016/S0040-1951(98)00289-3).
- Moretti, M., Soria, J.M., Alfaro, P., Walsh, N., 2001. Asymmetrical soft-sediment deformation structures triggered by rapid sedimentation in turbiditic deposits (Late Miocene, Guadix Basin, Southern Spain). *Facies* 44, 283–294. <https://doi.org/10.1007/BF02668179>.
- Moretti, M., Sabato, L., 2007. Recognition of trigger mechanisms for soft-sediment deformation in the Pleistocene lacustrine deposits of the sant' Arcangelo Basin (Southern Italy): seismic shock vs. overloading. *Sediment. Geol.* 196, 31–45. <https://doi.org/10.1016/j.sedgeo.2006.05.012>.
- Moretti, M., Van Loon, A.J., 2014. Restrictions to the application of ‘diagnostic’ criteria for recognizing ancient seismites. *J. Palaeogeogr.* 3, 162–173. <https://doi.org/10.3724/SP.J.1261.2014.00050>.
- Muir-Wood, R., 2000. Deglaciation seismotectonics: a principal influence on intrapllate seismogenesis at high latitudes. *Quat. Sci. Rev.* 19, 1399–1411. [https://doi.org/10.1016/S0277-3739\(00\)00069-X](https://doi.org/10.1016/S0277-3739(00)00069-X).
- Muschitello, F., Lea, J.M., Greenwood, S.L., Nick, F.M., Brunnberg, L., MacLeod, A., Wohlforth, B., 2016. Timing of the first drainage of the Baltic Ice Lake synchronous with the onset of Greenland Stadial 1. *Boreas* 45, 322–334. <https://doi.org/10.1111/bor.12155>.
- Nakai, K., 2005. An elasto-plastic constitutive modeling of soils based on the evolution laws describing collapse of soil skeleton structure. *Loss of Overconsolidation and Development of Anisotropy*. Nagoya University. Doctoral Thesis (in Japanese).
- Nartišs, M., Woronko, B., Pisarska-Jamrozy, M., Belzty, S., Bitinas, A., 2018. Injection structures and load casts in lagoon sediments (Sārnate outcrop, W Latvia). In: *Excursion guide & abstracts of International Palaeoseismological Field Workshop Lithuania*, pp. 32–37.
- Nettles, M., Ekström, G., 2010. Glacial earthquakes in Greenland and Antarctica. *Annu. Rev. Earth Planet Sci.* 38, 467–491. <https://doi.org/10.1146/annurev-earth-040809-152414>.
- Nikulin, V., 2011. Assessment of the seismic hazard in Latvia. Version of 2007 year. RTUžinātniskie raksti. Materiālzinātne un lietišķa ķīmija. Sērija 1, sejums 24, 110–115.
- Obermeier, S.F., 1996. Use of liquefaction-induced features for paleoseismic analysis – an overview. *Eng. Geol.* 44, 1–76. [https://doi.org/10.1016/S0013-7952\(96\)00040-3](https://doi.org/10.1016/S0013-7952(96)00040-3).
- Obermeier, S.F., 2009. Using liquefaction-induced and other soft-sediment features for paleoseismic analysis. In: McCalpin, J.P. (Ed.), *Paleoseismology*. Elsevier, New York, pp. 497–564. [https://doi.org/10.1016/S0074-6142\(09\)95007-0](https://doi.org/10.1016/S0074-6142(09)95007-0).
- Oliveira, C.M.M., Hodgson, D.M., Flint, S.S., 2011. Distribution of soft-sediment deformation structures in clinoform successions of the Permian Etca Group, Karoo Basin, South Africa. *Sediment. Geol.* 235, 314–330. <https://doi.org/10.1016/j.sedgeo.2010.09.011>.
- Owen, G., 1996. Experimental soft-sediment deformation: structures formed by the liquefaction of unconsolidated sands and some ancient examples. *Sedimentology* 43, 279–293. <https://doi.org/10.1046/j.1365-3091.1996.d01-5.x>.
- Owen, G., 2003. Load structures: gravity-driven sediment mobilization in the shallow subsurface. In: Van Rensbergen, R., Hillis, R.R., Maltman, A.J., Morley, C.K. (Eds.), *Subsurface Sediment Mobilization*, vol 216, pp. 21–34. <https://doi.org/10.1144/GSL.SP.2003.216.01.03>.
- Owen, G., Moretti, M., 2008. Determining the origin of soft-sediment deformation structures: a case study from Upper Carboniferous delta deposits in south-west Wales, UK. *Terra Nova* 20, 237–245. <https://doi.org/10.1111/j.1365-3121.2008.00807.x>.
- Owen, G., Moretti, M., 2011. Identifying triggers for liquefaction-induced soft-sediment deformation in sands. *Sediment. Geol.* 235, 141–147. <https://doi.org/10.1016/j.sedgeo.2010.10.003>.
- Owen, G., Moretti, M., Alfaro, P., 2011. Recognising triggers for soft-sediment deformation: current understanding and future directions. *Sediment. Geol.* 235, 133–140. <https://doi.org/10.1016/j.sedgeo.2010.12.010>.
- Passega, R., 1964. Grain size representation by CM patterns as a geological tool. *J. Sediment. Res.* 34, 830–847. <https://doi.org/10.1306/74D711A4-2B21-11D7-8648000102C1865D>.
- Passega, R., Byramjee, R., 1969. Grain-Size image of clastic deposits. *Sedimentology* 13, 233–252. <https://doi.org/10.1111/j.1365-3091.1969.tb00171.x>.
- Paškevičius, J., 1997. The geology of the Baltic republics. *Liet. Geol. Tarnyba* 387. Vilnius.
- Phillips, E., 2006. Micromorphology of a debris flow deposit: evidence of basal shearing, hydrofracturing, liquefaction and rotational deformation during emplacement. *Quat. Sci. Rev.* 25, 720–738. <https://doi.org/10.1016/j.quascirev.2005.07.004>.
- Phillips, E., van der Meer, J.J.M., Ferguson, A., 2011. A new ‘microstructural mapping’ methodology for the identification, analysis and interpretation of polyphase deformation within subglacial sediments. *Quat. Sci. Rev.* 30, 2570–2596. <https://doi.org/10.1016/j.quascirev.2011.04.024>.
- Phillips, E., Evans, D.J.A., van der Meer, J.J.M., Lee, J.R., 2018. Microscale evidence of liquefaction and its potential triggers during soft-bed deformation within subglacial traction tills. *Quat. Sci. Rev.* 181, 123–143. <https://doi.org/10.1016/j.quascirev.2017.12.003>.
- Phillips, E., Evans, D.J.A., 2019. Synsedimentary glaciectonic deformation within a glaciocastrine-esker sequence, Teesdale, Northern England. *Proc. Geol. Assoc.* 130, 624–649. <https://doi.org/10.1016/j.pgeola.2019.08.001>.

- Pisarska-Jamrozy, M., Zieliński, T., 2012. Specific erosional and depositional processes in a Pleistocene subglacial tunnel in the Wielkopolska region, Poland. *Geogr. Ann.* 94A, 429–443. <https://doi.org/10.1111/j.1468-0459.2012.00466.x>.
- Pisarska-Jamrozy, M., 2013. Varves and megavarves in the Eberswalde Valley (NE Germany) – a key for the interpretation of glaciolimnic processes. *Sediment. Geol.* 291, 84–96. <https://doi.org/10.1016/j.sedgeo.2013.03.018>.
- Pisarska-Jamrozy, M., Belzty, S., Börner, A., Hoffmann, G., Hüneke, H., Kenzler, M., Obst, K., Rother, H., Van Loon, A.J., 2018. Evidence from seismites for glacioisostatically induced crustal faulting in front of an advancing land-ice mass (Rügen Island, SW Baltic Sea). *Tectonophysics* 745, 338–348. <https://doi.org/10.1016/j.tecto.2018.08.004>.
- Pisarska-Jamrozy, M., Woźniak, P.P., 2019. Debris flow and glacioisostatic-induced soft-sediment deformation structures in a Pleistocene glaciolacustrine fan: the southern Baltic Sea coast, Poland. *Geomorphology* 326, 225–238. <https://doi.org/10.1016/j.geomorph.2018.01.015>.
- Pisarska-Jamrozy, M., Belzty, S., Bitinas, A., Jusinié, A., Woronko, B., 2019a. Seismic shocks, periglacial conditions and glacitectonics as causes of the deformation of a Pleistocene meandering river succession in central Lithuania. *Baltica* 32, 62–77.
- Pisarska-Jamrozy, M., Belzty, S., Börner, A., Hoffmann, G., Hüneke, H., Kenzler, M., Obst, K., Rother, H., Steffen, H., Steffen, R., Van Loon, A.J., 2019b. The sea cliff at Dwasieden: soft-sediment deformation structures triggered by glacial isostatic adjustment in front of the advancing Scandinavian Ice 1016 sheet. *E&G Quat. Sci. J.* 2, 61–64. <https://doi.org/10.5194/deuquasp-2-61-2019>.
- Pisarska-Jamrozy, M., Belzty, S., Börner, A., Hoffmann, G., Kenzler, M., Rother, H., Steffen, R., Steffen, H., 2022. Late Pleistocene earthquakes imprinted on glaciolacustrine sediments on Gnitz Peninsula (Usedom Island, NE Germany). *Quat. Sci. Rev.* 296, 107807. <https://doi.org/10.1016/j.quascirev.2022.107807>.
- Pisarska-Jamrozy, M., Woronko, B., Woźniak, P.P., Rosentau, A., Hang, T., Steffen, H., Steffen, R., 2024. Deformation structures as key hints for interpretation of ice sheet dynamics - a case study from northeastern Estonia. *Quat. Sci. Rev.* 365, 1–18. <https://doi.org/10.1016/j.quascirev.2024.108788>.
- Podolskiy, E.A., Walter, F., 2016. Cryoseismology. *Rev. Geophys.* 54, 708–758. <https://doi.org/10.1002/2016RG000526>.
- Potter, P.E., Pettijohn, F.J., 1977. *Paleocurrents and Basin Analysis*, second ed. Springer-Verlag, New York, p. 425.
- Ravier, E., Buoncristiani, J.-F., Guiraud, M., Menzies, J., Clerc, S., Goupy, B., Portier, E., 2014. Porewater pressure control on subglacial soft sediment remobilization and tunnel valley formation: a case study from the Alnif tunnel valley (Morocco). *Sediment. Geol.* 304, 71–95. <https://doi.org/10.1016/j.sedgeo.2014.02.005>.
- Ravier, E., 2024. Physical characteristics of hydrofracture systems and their fills in glacial sediments. *Sedimentology* 463, 106593. <https://doi.org/10.1016/j.sedgeo.2024.106593>.
- Reicherter, K., Michetti, A.M., Silva Barroso, P.V., 2009. Paleoseismology: historical and prehistorical records of earthquake ground effects for seismic hazard assessment. *Geol. Soc. Lond. Spec. Publ.* 316, 1–10. <https://doi.org/10.1144/SP316.1>.
- Rodríguez-Pascua, M.A., Calvo, J.P., De Vicente, G., Gomez-Gras, D., 2000. Soft-sediment deformation structures interpreted as seismites in lacustrine sediments of the Prebetic Zone, SE Spain, and their potential use as indicators of earthquake magnitudes during the Late Miocene. *Sediment. Geol.* 135, 117–135. [https://doi.org/10.1016/S0037-0738\(00\)00067-1](https://doi.org/10.1016/S0037-0738(00)00067-1).
- Rosentau, A., Vassiljev, J., Hang, T., Saarste, L., Kalm, V., 2009. Development of the Baltic ice Lake in the eastern Baltic. *Quat. Int.* 206, 16–23. <https://doi.org/10.1016/j.quaint.2008.10.005>.
- Rosentau, A., Grudzinska, I., Kalińska, E., Alexanderson, H., Bērziņš, V., Čeriņa, A., Kalniņa, L., Karuss, J., Lamsters, K., Muru, M., Nartīss, M., Paparde, L., Hang, T., 2023. Holocene relative shore-level changes and development of the Ķipka lagoon in the western Gulf of Riga. *Boreas* 52, 517–537. <https://doi.org/10.1111/bor.12628>.
- Saarnisto, M., Saarinen, T., 2001. Deglaciation chronology of the Scandinavian ice sheet from the Lake Onega Basin to the salpausselkä end moraines. *Global Planet. Change* 31, 387–405. [https://doi.org/10.1016/S0921-8181\(01\)00131-X](https://doi.org/10.1016/S0921-8181(01)00131-X).
- Saks, T., Kalvans, A., Zelcs, V., 2007. Structure and micromorphology of glacial and non-glacial deposits in coastal bluffs at Sensala, Western Latvia. *Baltica* 20, 19–27.
- Saks, T., Kalvans, A., Zelcs, V., 2011. Subglacial bed deformation and dynamics of the Apriķi glacial tongue, W Latvia. *Boreas* 41, 124–140. <https://doi.org/10.1111/j.1502-3885.2011.00222.x>.
- Saks, T., Kalvans, A., Zelcs, V., 2012. OSL dating of Middle Weichselian age shallow basin sediments in Western Latvia, Eastern Baltic. *Quat. Sci. Rev.* 44, 60–68. <https://doi.org/10.1016/j.quascirev.2010.11.004>.
- Saulite, A., Kalniņa, L., Stinkulis, G., Čeriņa, A., 2007. A new data from the outcrop at the coastal cliff of the Baltic sea near to Sārnate. In: Guobytė, R., Stancikaitė, M. (Eds.), *The Quaternary of Western Lithuania: from the Pleistocene Glaciations to the Evolution of the Baltic Sea: Proceedings: the INQUA Peribaltic Group Field Symposium, May 27-June 02, 2007, Plateliai, Lithuania*. Lithuanian Geological Survey, Institute of Geology and Geography, Vilnius, pp. 73–74.
- Seed, H.B., 1979. Soil liquefaction and cyclic mobility evaluation for level ground during earthquakes. *J. Geotech. Eng. Div.* 105, 201–255. <https://doi.org/10.1061/AJGEB.00000768>.
- Seed, H.B., Idriss, I.M., Arango, I., 1983. Evaluation of liquefaction potential using field performance data. *J. Geotech. Eng. Div.* 109, 458–482. [https://doi.org/10.1061/\(ASCE\)0733-9410\(1983\)109:3\(458](https://doi.org/10.1061/(ASCE)0733-9410(1983)109:3(458).
- Seidel, E., Steffen, H., Steffen, R., Ahlrichs, N., Hübscher, C., 2025. Drivers of glacially induced fault reactivation in the Baltic Sea sector of the Tornquist Fan. *Boreas*. <https://doi.org/10.1111/bor.12689>.
- Seilacher, A., 1969. Fault-graded beds interpreted as seismites. *Sedimentology* 13, 155–159. <https://doi.org/10.1111/j.1365-3091.1969.tb01125.x>.
- Shogenov, K., Shogenova, A., Vizika-Kavvadias, O., 2013. Potential structures for CO₂ geological storage in the Baltic Sea: case study offshore Latvia. *Bull. Geol. Soc. Finland* 85, 65–81. <https://doi.org/10.17741/bgsf/85.1.005>.
- Shogenova, A., Sliaupa, S., Vaher, R., Shogenov, K., Pomeranceva, R., 2009. The Baltic Basin: structure, properties of reservoir rocks and capacity for geological storage of CO₂. *Est. J. Earth Sci.* 58, 259–267. <https://doi.org/10.3176/earth.2009.4.04>.
- Sims, J.D., 1975. Determining earthquake recurrence intervals from deformational structures in young lacustrine sediments. *Tectonophysics* 29, 141–152. [https://doi.org/10.1016/0040-1951\(75\)90139-0](https://doi.org/10.1016/0040-1951(75)90139-0).
- Smith, N.D., Ashley, G., 1985. Proglacial lacustrine environments. In: Ashley, G., Shaw, J., Smith, N.D. (Eds.), *Glacial Sedimentary Environments*, vol. 16. Society of Economic Paleontologists and Mineralogists Short Course, pp. 135–216. <https://doi.org/10.2110/scn.85.02.0135>.
- Stárková, M., Martínek, K., Mikuláš, R., Rosenau, N., 2015. Types of soft-sediment deformation structures in a lacustrine Ploužnice member (Stephanian, Gzhelian, Pennsylvanian, Bohemian Massif), their timing, and possible trigger mechanism. *Int. J. Earth Sci.* 104, 1277–1298. <https://doi.org/10.1007/s00531-015-1155-5>.
- Steffen, H., Steffen, R., Tarasov, L., 2019. Modelling of glacially-induced stress changes in Latvia, Lithuania and the Kaliningrad District of Russia. *Baltica* 32, 78–90. <https://doi.org/10.5200/baltica.2019.1.7>.
- Stewart, I.S., Sauber, J., Rose, J., 2000. Glacioseismotectonics: ice sheets, crustal deformation and seismicity. *Quat. Sci. Rev.* 19, 1367–1389. [https://doi.org/10.1016/S0277-3791\(00\)00094-9](https://doi.org/10.1016/S0277-3791(00)00094-9).
- Stolarski, F., 1979. Powstanie lokalnych form tektonicznych w polskiej części synklinazy perybaltyckiej na tle rozwoju geologicznego całej jednostki [Formation of local structural forms in the Polish part of the Peri-baltic Syncline in the background of the geological development of the whole unit]. *Acta Geol. Pol.* 29, 519–559 (in Polish with English summary).
- Stroeven, A.P., Hätestrand, C., Kleman, J., Heyman, J., Fabel, D., Fredin, O., Goodfellow, B.W., Harbor, J.M., Jansen, J.D., Olsen, L., Caffee, M.W., Fink, D., Lundqvist, J., Rosqvist, G.C., Strömborg, B., Jansson, K.N., 2016. Deglaciation of fennoscandia. *Quat. Sci. Rev.* 147, 91–121. <https://doi.org/10.1016/j.jgs.2015.09.016>.
- Sumer, B.M., Hatipoglu, F., Fredsøe, J., Sumer, S.K., 2006. The sequence of sediment behaviour during wave-induced liquefaction. *Sedimentology* 53, 611–629. <https://doi.org/10.1111/j.1365-3091.2006.00763.x>.
- Suveizdis, P., Brangulis, A., Puura, V., Brio, Ch., Laškovas, E., 1979. Structure of a sedimentary cover. *Baltic Tectonics* 41–50.
- Sliaupa, S., Hoth, P., 2011. Geological evolution and resources of the Baltic Sea area from the Precambrian to the Quaternary. In: *The Baltic Sea Basin*, pp. 13–53. https://doi.org/10.1007/978-3-642-17220-5_2.
- Świątek, S., Belzty, S., Pisarska-Jamrozy, M., Woronko, B., 2023. Sedimentary records of liquefaction: implications from field studies. *J. Geophys. Res. Earth Surf.* 128, e2023JE007152. <https://doi.org/10.1029/2023JE007152>.
- Świątek, S., Lewińska, K., Pisarska-Jamrozy, M., Günther, C., 2025. An application of quartz grain analyses in earthquake-induced (palaeo)liquefaction studies. *J. Struct. Geol.* 193, 105357. <https://doi.org/10.1016/j.jsg.2025.105357>.
- Świątek, S., Pisarska-Jamrozy, M., 2025. Seismogenic liquefaction with M~3.5 in fine-grained sediments: an experimental approach. *Sediment. Geol.* 478, 106833. <https://doi.org/10.1016/j.sedgeo.2025.106833>.
- Tang, X.W., Hu, J.L., Qiu, J.N., 2016. Identifying significant influence factors of seismic soil liquefaction and analyzing their structural relationship. *J. Civ. Eng.* 20, 2655–2663. <https://doi.org/10.1007/s12205-016-0339-2>.
- Taylor, B.J., 1982. Sedimentary dykes, pipes and related structures in the Mesozoic sediments of south-eastern Alexander Island, Antarctica. *Br. Antarct. Surv. Bull.* 51, 1–42.
- Tikkakan, M., Oksanen, J., 2002. Late Weichselian and Holocene shore displacement history of the Baltic Sea in Finland. *Fennia* 180, 9–20.
- Tsai, V.C., Rice, J.R., Fahnestock, M., 2008. Possible mechanisms for glacial earthquakes. *J. Geophys. Res.* 113, F03014. <https://doi.org/10.1029/2007JF000944>.
- Tuuling, I., 2019. The Leba Ridge-Riga-Pskov Fault Zone—a major East European Craton interior dislocation zone and its role in the early Palaeozoic development of the platform cover. *Est. J. Earth Sci.* 68, 161–189. <https://doi.org/10.3176/earth.2019.12>.
- Üner, S., Sağlam Selçuk, A., Özsayın, E., 2019. Non-seismic soft-sediment deformation structures from Late Pleistocene lacustrine deposits of Lake Van (Eastern Turkey): storm and overloading effect. *J. Great Lake. Res.* 45, 664–671. <https://doi.org/10.1016/j.jglr.2019.03.007>.
- Uyanık, O., Ekinci, B., Uyanık, N.A., 2013. Liquefaction analysis from seismic velocities and determination of Lagoon Limits Kumluca/Antalya example. *J. Appl. Geophys.* 95, 90–103.
- van der Meer, J.J.M., Menzies, J., 2011. The micromorphology of unconsolidated sediments. *Sediment. Geol.* 238, 213–232.
- van der Meer, J.J.M., Kjær, K.H., Krüger, J., Rabassa, J., Kilfeather, A.A., 2009. Under pressure: clastic dykes in glacial settings. *Quat. Sci. Rev.* 28, 708–720. <https://doi.org/10.1016/j.jgs.2008.07.017>.
- Van Loon, A.J., 2009. Soft-sediment deformation structures in siliciclastic sediments: an overview. *Geologos* 15, 3–55.
- Van Loon, A.J., Pisarska-Jamrozy, M., 2014. Sedimentological evidence of Pleistocene earthquakes in NW Poland induced by glacioisostatic rebound. *Sediment. Geol.* 300, 1–10. <https://doi.org/10.1016/j.sedgeo.2013.11.006>.
- Van Loon, A.J., Pisarska-Jamrozy, M., Nartīss, M., Krievāns, M., Soms, J., 2016. Seismites resulting from high-frequency, high-magnitude earthquakes in Latvia caused by Late Glacial glacio-isostatic uplift. *J. Palaeogeogr.* 5, 363–380. <https://doi.org/10.1016/j.jop.2016.05.002>.

- Van Loon, A.J., Pisarska-Jamrozy, M., Woronko, B., 2020. Sedimentological distinction in glaciogenic sediments between load casts induced by periglacial processes from those induced by seismic shocks. *Geol. Q.* 64, 626–640. <https://doi.org/10.7306/gq.1546>.
- Vanneste, K., Meghraoui, M., Camelbeeck, T., 1999. Late Quaternary earthquake-related soft-sediment deformation along the Belgian portion of the Feldbiss Fault, Lower Rhine Graben system. *Tectonophysics* 309, 57–79. [https://doi.org/10.1016/S0040-1951\(99\)00132-8](https://doi.org/10.1016/S0040-1951(99)00132-8).
- Van Vliet-Lanoë, B., Magyari, A., Meilliez, F., 2004. Distinguishing between tectonic and periglacial deformation of Quaternary continental deposits in Europe. *Global Planet. Change* 43, 103–127. <https://doi.org/10.1016/j.gloplacha.2004.03.003>.
- Varna, I., Haritonova, D., Balodis, J., 2019. Velocity fields of the Latvian CORS station daily coordinates for 2012–2017. *Geophysica* 54, 137–144.
- Vassiljev, J., Saarse, L., Rosentau, A., 2011. Palaeoreconstruction of the Baltic ice Lake in the Eastern Baltic. In: Harff, J., Björck, S., Hoth, P. (Eds.), *The Baltic Sea Basin*. Springer, pp. 189–202. <https://doi.org/10.1007/978-3-642-17220-5-9>.
- Vassiljev, J., Saarse, L., 2013. Timing of the Baltic Ice Lake in the eastern Baltic. *Bull. Geol. Soc. Finland* 85, 9–18.
- Weinbergs, I., 1979. The Quaternary history of the Baltic. Latvia. In: Gudelis, V., Königsson, L.K. (Eds.), *The Quaternary History of the Baltic. Acta Universitatis Upsaliensis, Uppsala*, pp. 147–157.
- Voisey, C.R., Hunter, N.J.R., Tomkins, A.G., Brugger, J., Liu, W., Liu, Y., Luzin, V., 2024. Gold nugget formation from earthquake-induced piezoelectricity in quartz. *Nat. Geosci.* 17, 920–925. <https://doi.org/10.1038/s41561-024-01514-1>.
- Wahyudi, S., Koseki, J., Sato, T., Miyashita, Y., 2013. Effects of pre-shearing history on repeated liquefaction behaviour of sand using stacked-ring shear apparatus. *Bullet. Earthquake Res. Soc.* 46, 3–11.
- Walker, R.G., Plint, A.G., 1992. Wave-and storm-dominated shallow marine systems. In: Walker, R.G., James, N.P. (Eds.), *Facies Models: Response to Sea Level Change*. Geological Association of Canada, Newfoundland, pp. 219–238.
- Walter, F., Olivieri, M., Clinton, J.F., 2013. Calving event detection by observation of seiche effects on the Greenland fjords. *J. Glaciol.* 59, 162–178.
- Wang, W.S., 1979. Some findings in soil liquefaction. *Earthquake Engineering Department, Water Conservancy and Hydroelectric Power Scientific Research Institute*, p. 17.
- Woźniak, P.P., Belzyt, S., Pisarska-Jamrozy, M., Woronko, B., Lamsters, K., Nartišs, M., Bitinas, A., 2021. Liquefaction and re-liquefaction of sediments induced by uneven loading and glaciogenic earthquakes: implications of results from the Latvian Baltic Sea coast. *Sediment. Geol.* 421, 105944. <https://doi.org/10.1016/j.sedgeo.2021.105944>.
- Xu, S., Hao, F., Xu, C., Wang, Y., Zou, H., Gong, C., 2015. Differential compaction faults and their implications for fluid expulsion in the northern Bohzhong Subbasin, Bohai Bay Basin, China. *Mar. Petrol. Geol.* 63, 1–16. <https://doi.org/10.1016/j.marpetgeo.2015.02.013>.
- Yang, R., Van Loon, A.J., Yin, W., Fan, A., Han, Z., 2016. Soft-sediment deformation structures in cores from lacustrine slurry deposits of the Late Triassic Yanchang Fm. (central China). *Geologos* 22, 201–211. <https://doi.org/10.1515/logos-2016-0021>.
- Youd, T.L., 1973. Liquefaction, Flow, and Associated Ground Failure, vol. 688. USGS Circular. <https://doi.org/10.3133/cir688>.
- Zelčs, V., Markots, A., Nartišs, M., Saks, T., 2011. Pleistocene glaciations in Latvia. In: Ehlers, J., Gibbard, P.L., Hughes, P.D. (Eds.), *Quaternary Glaciations – Extent and Chronology: a Closer Look, Developments in Quaternary Science*, vol. 15, pp. 221–229. Amsterdam.
- Zelčs, V., Nartišs, M., 2014. Outlines of the Quaternary geology of Latvia. Excursion Guide and Abstracts of the INQUA Peribaltic Working Group Meeting and Field Excursion in Eastern and Central Latvia. University of Latvia, August, pp. 17–22. <https://doi.org/10.22364/lqpsn.2014.16>.
- Zen, K., Yamazaki, H., 1990. Mechanism of wave-induced liquefaction and densification in seabed. *Soils Found.* 30, 90–104. <https://doi.org/10.3208/sandf1972.30.4.90>.
- Zieliński, T., Pisarska-Jamrozy, M., 2012. Jaki cechy litologiczne osadów warto kodować, a jakie nie? [Which features of deposits should be included in a code and which not?] *Prz. Geol.* 60, 387–397 (in Polish with English abstract).